Russian Chemical Reviews **81** (12) 1091 – 1116 (2012) © 2012 Russian Academy of Sciences and Turpion Ltd

DOI 10.1070/RC2012v081n12ABEH004285

Production of nanodispersed materials and thin films by laser ablation techniques in liquid and in vacuum

Yu S Tveryanovich, A A Manshina, A S Tverjanovich

Contents

I. Introduction 1091
II. Production of dispersed materials by laser ablation in liquid 1091
III. Laser ablation in vacuum: thin film deposition 1101
IV. Conclusion 1113

Abstract. The methods of laser ablation of chemical compounds in a liquid medium and in vacuum used for the production of highly dispersed materials and films, respectively, are considered. Features and advantages of these methods are noted and the potential of their application for the design of novel materials is discussed. Examples of application of these methods in scientific research are given. The bibliography includes 177 references.

I. Introduction

Laser ablation is used more and more often to obtain new materials. Two key areas of the development of laser ablation can be distinguished, namely, laser ablation in liquid (LAL) and laser ablation in vacuum (LAV). For chemistry, of particular interest is the possibility of producing nanodispersed materials (by LAL) and film materials (by LAV).

A laser pulse delivers high fluence, which results in the formation of plasma. According to formal estimates, the plasma temperature is about thousands of degrees. Also, it appears possible to obtain nanodispersed systems and films that retain the elemental composition and the structure of the target. This possibility is ensured by the pronounced deviation of the laser-ablation process conditions from thermodynamic equilibrium. During the laser ablation in vacuum, the laser plume contains not only ions and atoms but also clusters of various size (up to microscopic droplets) in which the target chemical structure is retained. When condensing on the substrate, these clusters can serve as phase nuclei, the chemical structure of the ablated compound being restored around them.

The matrix-assisted pulse laser evaporation (MAPLE) technique is used successfully for laser deposition of complex organic compounds.† It is worthy of note that during ablation of organic compounds in liquid, they can be transferred to the nanodispersed state without generation of considerable amounts of decomposition products (see below). Also, with appropriate selection of the material being ablated and the liquid, laser dispersion process can be combined with the chemical reaction needed to prepare the desired compound in highly dispersed state.

This review presents analysis of publications of the last decade devoted to ablation of chemical compounds in vacuum and in liquid media.‡

II. Production of dispersed materials by laser ablation in liquid

1. Scope of application of nanomaterials produced by laser ablation in liquid

Laser ablation in liquid can be used to produce numerous nanodispersed materials applied in various fields.

The LAL technique was used to obtain silver selenide.[1] This compound is a superionic conductor widely utilized in solar cell elements and as an optical filter.[2] Nanodispersed solid electrolytes for accumulator batteries such as $LiCoO_2$ (Ref. 3) and $LiMn_2O_4$ are prepared by LAL.[4]

The LAL method is also used for the design of other oxide materials. The ablation of the appropriate ceramics in deionized water gave 10 – 30 nm nanoparticles of $CaMoO_4$.[5] Nanoparticles of the same composition and $CaWO_4$ nanoparticles were obtained by ablation in ethanol.[6] In both cases, fourth harmonic radiation from the Nd : YAG laser

Yu S Tveryanovich, A A Manshina, A S Tverjanovich Department of Chemistry, Saint Petersburg State University, Universitetsky prosp. 26, 198504 St Petersburg, Petrodvorets, Russian Federation.
Fax (7-812) 428 67 33,
tel. (7-812) 428 74 79, e-mail: tys@bk.ru (Yu S Tveryanovich),
tel. (7-812) 428 43 35, e-mail: alina_manshina@mail.ru (A A Manshina),
tel. (7-812) 428 40 84, e-mail: andr.tver@yahoo.com (A S Tverjanovich)

Received 10 November 2011
Uspekhi Khimii **81** (12) 1091 – 1116 (2012); translated by Z P Svitanko

† For more details of the process, see for example A L Mercado, C E Allmond, J G Hoekstra, J M Fitz-Gerald *Appl. Phys. A* **81** 591 (2005).

‡ The review does not consider the ablation of metals and various carbon polymorphs in liquids, which is widely covered in the literature and, for example, forms the subject of the detailed review G W Yang *Prog. Mater. Sci.* **52** 648 (2007).

was used [wavelength (λ) 266 nm, pulse duration (τ_p) 8 ns, pulse energy (E_p) up to 100 mJ]. The authors noted that these nanoparticles can be used as blue luminescence media,[7–9] laser media for electronics,[10–12] scintillators in medicine[13–15] and media for masers.[16,17] Nanoparticles of $Sr_2MgSi_2O_7:Eu^{2+},Dy^{3+}$, which is a well-known luminophore, with long luminescence, were obtained.[18]

The LAL technique served to obtain Bi_2O_3 nanoparticles,[19] which are suitable as photocatalysts, as was demonstrated for photooxidation of an aqueous solution of indigo. It was confirmed experimentally that the catalytic activity of nanodispersed bismuth oxide is higher than that of microdispersed one. Ablation was performed by a femtosecond laser (λ = 800 nm, τ_p = 120 fs, E_p = 0.5 mJ).

Tsuji *et al.*[20] ablated cobalt and cobalt oxides, CoO (used in chemical sensors[21]) and Co_2O_3, in various liquid media.

Nanocrystalline luminophores were prepared by ablation of Gd_2O_3 ceramics doped with erbium and ytterbium.[22] The luminescence spectra of these luminophores displayed bands corresponding to two- and three photon excitation of erbium ions. Presumably, they will find use as luminescent markers in biological and medical research. Effective luminophores $Gd_2SiO_5:Ce^{3+}$ and $Lu_2O_2S:Eu^{3+}$ with grain size of 1–5 nm were produced by the LAL method.[23]

Indium ablation in water gave[24] nanoparticles of indium oxide, which is a unique transparent compound with high conductivity used in the upper conducting layers of battery solar cells or displays and in active layers of resistive chemical sensors for ozone, CO and NO_2.[25–27] It was shown§ that CO sensors based on colloid solutions of indium oxide prepared by LAL have good performance and are able to detect <2 ppm of carbon monoxide, the speed of response being several seconds.

Successive ablation of magnesium (or zinc) and then aluminium in deionized water afforded[28] stoichiometric nanocrystals of layered double hydroxides, $Mg_6Al_2(OH)_{18}\cdot 4.5H_2O$ and $Zn_6Al_2(OH)_{18}\cdot 4.5H_2O$, which can absorb undesirable impurities from gas and liquid media. Also, materials with unusual rheological properties can be formed from these compounds.

Nanodispersed semiconductors or their colloid solutions are used as nonlinear optical materials.[29] Ganeev and Ryasnyansky[30] prepared nanodispersed sulfides CdS and As_2S_3 with a mean particle size of 2 and 4 nm, respectively. In both cases, the fundamental absorption edge shifts to shorter wavelength (the initial As_2S_3 and its nanodispersed particles were glass-like solids). According to estimates,[30] the optical nonlinearity of nanodispersed particles is 2–3 orders of magnitude greater in the absolute value than the optical nonlinearity of bulky materials. The same conclusion was drawn by Ganeev *et al.*,[31] who considered Ge and GaAs nanoparticles. However, they failed to obtain a stable colloid solution with a high concentration of these particles.

The nanocrystalline semiconductors obtained by LAL, for example, CdS and GaAs, are also studied as luminescent materials.[32] The LAL process is suitable for producing luminescent semiconductor particles whose luminescence spectrum spans the visible range up to blue luminescence in silicon nanocrystals.[33]

The LAL-produced nanodispersed InP with crystal size of up to 100 nm is considered as a material for optoelectronics and biomedicine.[34] The attention was drawn to PbTe, as it has a narrow bandgap (0.32 eV) and a large exciton Bohr radius (46 nm). This implies that the size effect should be manifested even for rather coarse particles. This material is promising for solar-battery cells,[35–37] telecommunication systems,[38] field effect transistors[39] and for the generation of thermoelectricity and enhancement of the image contrast in microbiological research.[40]

Laser ablation is an efficient method for the synthesis of various carbon structures, for example, fullerenes,[41] carbon nanotubes,[42] polyynes described as $H-(C\equiv C)_n-H$.[43] The polyynes are used to design one-dimensional conductors; they can also be utilized to form other carbon structures. Attempts to prepare polyynes by the LAL technique were made in several works.[44–47] Tabata *et al.*[47] performed the synthesis with the use of colloid solutions of 5 nm diamond and graphite particles in ethanol. The second harmonic of the Nd:YAG laser was used [λ = 532 nm, τ_p = 7 ns, radiation fluence (ρ_E) 1.3 J cm^{-2}]. This gave polyynes up to n = 16. When diamonds were used as precursors, the average chain length in the products of synthesis increased. For coarser diamond particles, the yield increased, but, as in the case of long-term laser irradiation, the average length of polyyne molecules decreased.[46]

Yet another group of materials obtained by LAL comprises organic compounds.[48–52] Despite the formation of some decomposition products, it is possible to preserve the chemical structure of the ablated compounds. By means of the LAL method, one can prepare colloid solutions of nanoparticles of insoluble organic compounds in order to form films and to use these solutions for the subsequent pharmacological synthesis.[48] For example, perylene-3,4,9,10-tetracarboxylic dianhydride exhibits semiconductor properties owing to the extended π-bond system.[48] More intricate, for example, biological items can also be ablated. Calcium phosphate nanoparticles were produced by ablation of fish bones without precalcination[53] and hydroxyapatite nanoparticles were obtained by ablation of precalcined fish bones.[54] Both these materials (especially hydroxyapatite) are successfully used in orthopaedy and prosthetic dentistry.[55] The ablation in deionized water by a CO_2 laser [λ = 10.6 μm, τ_p = 10 μs, ν = 10–16 kHz, E_p = 2–2.52 mJ, $\rho_W = (1-1.4)\times 10^6$ W cm^{-2}, W = 100 W; here and below ν is the pulse repetition rate, ρ_w is the pulse power density, W is the average radiation power] gave the hydroxyapatite nanoparticles from the synthetic bulk material.[55] When ablation was carried out for calcined fish bones, the nanoparticles thus formed contained the tricalcium phosphate phase in addition to the hydroxyapatite. The tricalcium phosphate nanoparticles are of particular interest as they are biodegradable and, hence, they are used as bone implant components to be subsequently replaced by natural bone tissue and for targeted drug delivery. These studies were continued and it was concluded[56] that hydroxyapatite is converted to tricalcium phosphate owing to the high temperatures during laser ablation.

The above list of ablated compounds and practical applications of the resulting materials clearly demonstrates

§ N Donato, F Neri, G Neri, M Latino, F Barreca, S Spadaro, I Pisagatti, G Curro *Thin Solid Films* **520** 922 (2011).

the versatility of the LAL method for the production of a variety of nanodispersed materials.

2. Characteristic features of laser ablation in liquid and model concepts

The advantages of the LAL method include[40] environmental friendliness, in particular, owing to the absence of by-products; availability of the starting materials; the possibility of preserving the chemical composition of the target; no need of vacuum or high temperatures and pressures. The preparation of colloid solutions by LAL, unlike traditional chemical methods, does not require auxiliary (often corrosive) reagents.

A specific feature of LAL is that expansion of laser-induced plasma is held back by the condensed medium. This leads to generation of a shock wave and local pressure and temperature buildup.[40] According to examination of the emission spectra of the plasma C_2 molecules formed upon exposure of a graphite target to Nd : YAG laser pulses (λ = 1064 nm, τ_p = 20 ns, ρ_E = 10 J cm^{-2}) in water, the plasma temperature was 5000 K.[57]

The following data about the pressure achieved in the ablation area are available. When laser pulses (λ = 1064 nm, τ_p of several tens of nanoseconds, ρ_W = 10 GW cm^{-2}) act on an aluminium target immersed in water, the pressure in the laser torch is 5.5 GPa.[58] A plasma-induced pressure of up to 2–2.5 GPa achieved upon irradiation of aluminium in water with an excimer laser (λ = 308 nm, τ_p = 50 ns, ρ_W = 1–2 GW cm^{-2}) was reported.[59] According to another publication,[60] an increase in the pulse duration from 3 to 30 ns results in decrease in the maximum pressure from 10 to 5 GPa.

The fact that high pressures may be achieved in the laser plasma confined by a liquid medium indicates the possibility of nanodiamond synthesis by LAL upon irradiation of graphite by Nd : YAG laser pulses (λ = 532 nm) in water[61,62] or acetone.[63] It is known that diamonds are formed only at fairly high pressures and temperatures. It was reported[58] that at 4500 K and 10 Gpa, the critical size of the diamond nucleus is 10 nm. The cited study considers specific aspects of the LAL method.[58]

Of no less importance is fast cooling of the ablated material by the surrounding liquid. Saito *et al.*[64] reported comparative results of high-speed shooting of laser plasma in water and in air (Fig. 1). It was concluded that the plasma lifetime (t) is an order of magnitude longer in air. However, it is necessary to take into account not only the plasma lifetime but also the kinetics of the development of plasma. In this respect, comparison of the photographic images reveals an even more surprising result. Whereas for ablation in the gas medium, the plasma luminescence reaches a maximum at $t \approx 300$ ns, for the ablation in liquid, the luminescence intensity maximum cannot be detected as it is attained in less than 21 ns (Fig. 2). Thus, cooling of the plasma starts almost immediately after the pulse is over.

It was noted[34] that high volatility of phosphorus is a severe problem in the preparation of InP nanoparticles by ablation. The authors expected that during LAL, high pressure in a bubble will restrict the evaporation of phosphorus and the fast cooling of the ablation products will stop this undesirable process. They actually were able to obtain indium phosphide nanocrystals contaminated with indium oxide by ablation in water. They used a nitrogen laser (λ = 337 nm, τ_p = 10 ns, ν = 10 Hz, E_p = 7 mJ, focal spot diameter 100 μm). Nanodispersed InP was obtained[65] by ablation in ethanol using Nd : YAG laser radiation with Q factor modulation. The laser radiation power was $<$0.5 mW. Two wavelengths were used, 266 and 532 nm. In the former case, due to a great radiation absorption coefficient, smaller particles were formed (2–3 nm) and the cooling rate was higher (according to authors' estimates, 1.5×10^{18} K s^{-1}). The particles did not have time to form the crystal structure. When radiation at λ = 532 nm was used, particles with up to 10 nm size and clear-cut crystal structure were formed. The cooling rate was estimated to be three orders of magnitude lower in this case. For estimation, the following expression was used:[66]

$$\left.\frac{\Delta T}{\Delta t}\right|_{\text{cooling}} = \frac{(1-R)W\alpha^3\tau_p 2D}{\rho C_p}$$

where R is the reflection coefficient, α is the light absorption coefficient, D is the thermal diffusion coefficient, ρ is the substance density, C_p is the substance heat capacity. It was assumed that heat diffusion occurs by the distance α^{-1} and that this requires time $\alpha^{-2}/2D$.

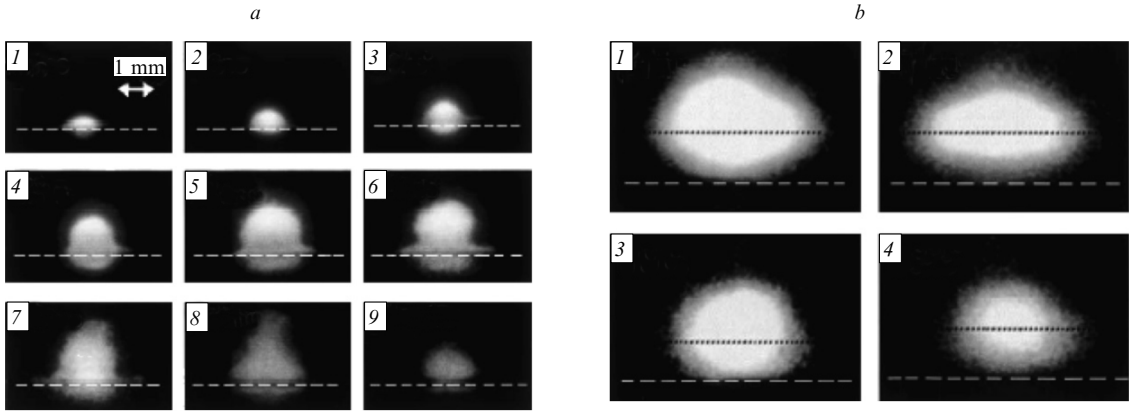


Figure 1. Variation of the laser plasma luminescence intensity after the action of a pulse from a Nd : YAG laser (λ = 1064 nm, τ_p = 20 ns, ρ_E = 10 J cm^{-2}) on a graphite target in air (*a*) and in water (*b*).[64]
(*a*) t/ns: (*1*) 21, (*2*) 46, (*3*) 56, (*4*) 86, (*5*) 256, (*6*) 356, (*7*) 556, (*8*) 756, (*9*) 1080; (*b*) t/ns: (*1*) 21, (*2*) 40, (*3*) 60, (*4*) 80.

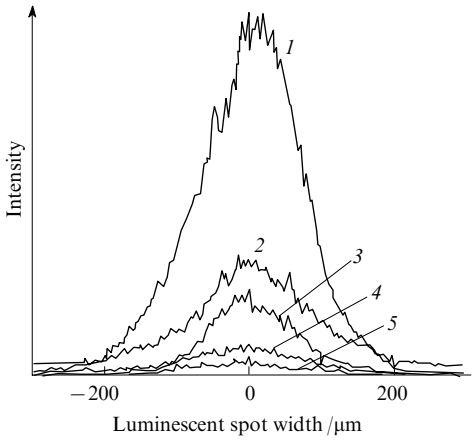


Figure 2. Variation of the laser-induced plasma luminescence intensity after the action of a pulse from a Nd:YAG laser (λ = 1064 nm, τ_p = 20 ns, ρ_E = 10 J cm^{-2}) on a graphite target in water.[64]
t /ns: (*1*) 21, (*2*) 40, (*3*) 60, (*4*) 80, (*5*) 100.

The features of LAL and the models that describe it can be grasped and verified by comparing the effects of laser pulses in liquid and gas media. Liu *et al.*[67] compared the results of treating monolithic silicon surfaces with femtosecond laser pulses in various media (water, ethanol, air). Liquid medium was found to enhance the ablating effect of laser pulses. Analogous studies of silicon ablation in various media were carried out by other researchers.[68, 69] They used a titanium sapphire laser (λ = 800 nm). The pulse duration and repetition frequency were several femtoseconds and 1 kHz, respectively, while the pulse energy varied continuously. The differences between the ablation results in different media are demonstrated in Fig. 3. First of all, attention is drawn by the smoothness of the crater walls and larger size of the craters formed upon ablation in the liquid medium. This is attributable to the above-noted restriction to the expansion of laser plasma by the medium, resulting in shock wave generation and pressure and temperature buildup in the local area. Presumably, the shock wave carries away the ablation products to the liquid medium, thus preventing them from deposition on the surface being ablated. The higher efficiency of ablation in liquid was quantitatively characterized in the following way. First, the authors approximated, as described in the literature,[70] the variation of the crater diameter (D) squared *vs.* the pulse energy by the linear dependence

$$D^2 = 2\,\omega_0^2 \ln\left(\frac{E_p}{E_{th}}\right)$$

where ω_0 is the beam radius in the focal plane, E_{th} is the threshold energy above which the ablation starts. The threshold fluence was determined from the equation

$$F_{th} = \frac{2\,E_{th}}{\pi\omega_0^2}$$

This parameter was found to be 1.3 – 1.4 higher in air than in the liquid medium. This was attributed, to some extent, to the fact that, according to authors' calculations, the reflection losses of the incident beam energy are lower by 9% in the liquid medium. Attention was drawn to one more property of the medium, which may affect the productivity of the LAL method: as a femtosecond pulse runs through ethanol, the intensity of supercontinuum generation is an order of magnitude higher than in the case of this pulse

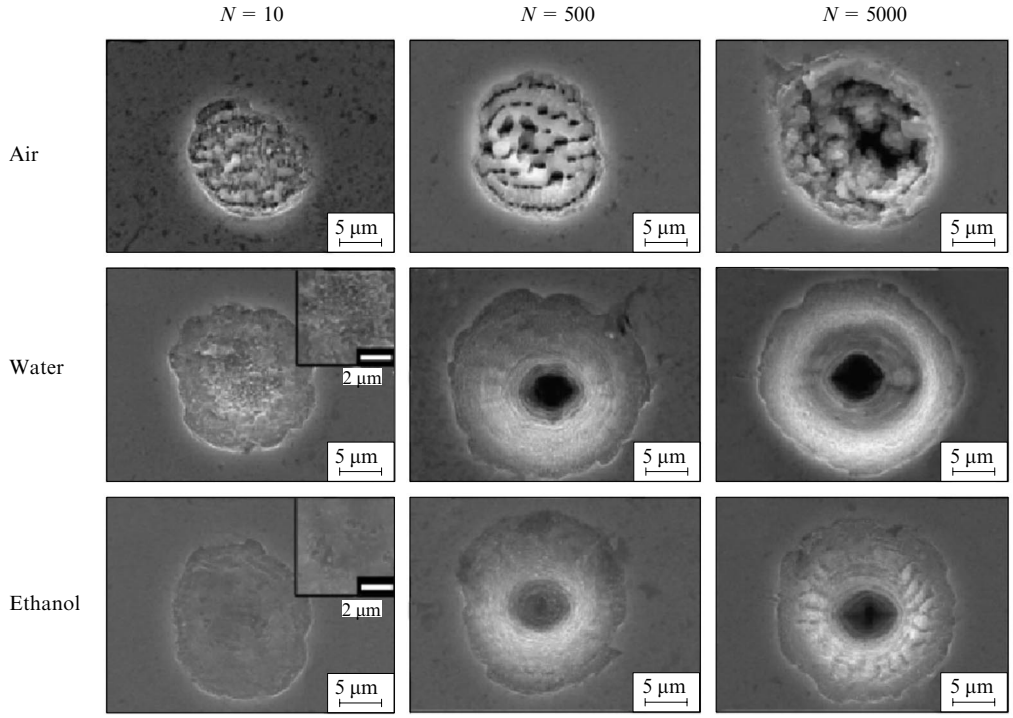


Figure 3. Photomicrographs of the craters formed upon ablation of silicon in various media at different pulse numbers (N) (E_p = 2.5 μJ).[67]

running through water. The authors believe that the energy lost for supercontinuum generation is a reason for lower efficiency of ablation in ethanol than in water.

Two mechanisms of nanoparticle formation are discussed in a paper [56] devoted to the ablation of hydroxyapatite in the aqueous medium. According to one of them, a laser beam heats a thin surface layer of the target until it melts. The target melting point is much higher than the boiling point of water and bubbles of the superheated steam tear the melt into spherical nanodrops, which are rapidly cooled in the aqueous medium. The second mechanism is mainly applicable, in the authors' opinion, to materials with low heat conductivity. In this case, if the power of the laser pulse is sufficient, the formed melt is strongly locally overheated and expands with explosion, not only melt drops but also crystalline fragments of the target being discharged to the environment. In terms of these views, it is possible to explain the retention of complex organic molecules upon ablation in the liquid medium. Indeed, it is not appropriate to restrict all processes that accompany laser ablation to generation of high temperatures and pressures. This is indicated, for example, by the following fact. The perylene-3,4,9,10-tetracarboxylic acid anhydride microcrystals were successfully dispersed down to sizes of tens of nanometres without changes in their chemical structure (perylene and C_8, C_{10}, C_{12} and C_{14} polyynes formed as by-products).[48]

The ablation of $CaMoO_4$ and $CaWO_4$ ceramic targets by the Nd : YAG laser fourth harmonics in ethanol was carried out.[6] The following assumption was made: if several laser pulses hit one and the same point of the target, a bubble of about micrometre in size, *i.e.*, much larger than the nanoparticles, can be formed from the ethanol vapour. Hence, ablation takes place to the gas medium. However, it should be borne in mind that the formation of a gas bubble of this size may essentially decrease the energy of laser radiation that hits the site of bubble attachment to the target as a result of defocusing.

An interesting observation was made by researchers [71] who performed ablation of titanium in deionized water induced by IR radiation ($\lambda = 1064$ nm, $\tau_p = 10.4$ ps, $E_p = 4$ μJ at $\nu = 50$ Hz, which corresponds to $W =$ 200 mW). They found that some of the formed spherical titanium monoxide particles have voids (Fig. 4). This was attributed (see also Refs 72 and 73) to the fact that the nucleation and condensation of the ablated substance occur at the interface between the liquid and gas bubbles, and this diminishes the interface free energy. Note that this interpretation does not coincide with the generally accepted view that spherical particles are formed from drops of the melt. Then the voids may have appeared in the following way. A spherical drop of the melt is rapidly cooled down due to heat removal from the surface. As a result, a void appears inside the drop. For the void volume to be one-eighth of the sphere volume (as shown in Fig. 4), the drop volume should be set constant (be coated by a solid crust) when the temperature inside the main bulk of the melt (T_0) is 1500°C higher than the melting point ($T_l = 2150$ K). Let the drop diameter be $2r = 100$ nm. The energy flux density through the drop surface at some instant of time during drop cooling can be expressed in two ways. On the one hand, this is energy given off by the drop as it is cooled by dT degrees in time dt (for simplicity, assume that the variable T runs over values from T_0 to 0) divided by the

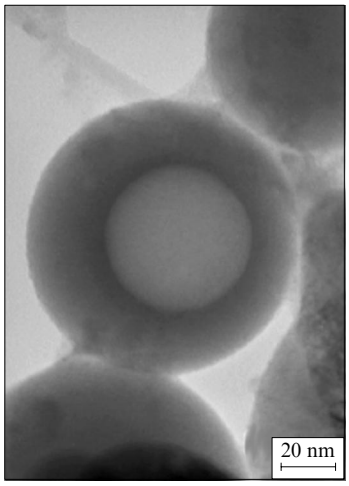


Figure 4. Photomicrograph of a hollow TiO particle.[71]

drop surface area (S) and, on the other hand, this is the product of substance heat conductivity by the temperature gradient

$$\frac{CV\rho dT}{S dt} = K\frac{T(t)}{r}$$

C is the specific heat capacity (~ 800 J kg^{-1} K^{-1}), V is the particle volume,

$$V = \frac{1}{3}rS$$

ρ is the substance density (~ 2000 kg m^{-3}), S is the particle specific surface area, t is the cooling time, K is the heat conductivity (~ 1 W K^{-1} m^{-1}).

From this, we found that

$$\ln\frac{T_0}{T_l} = \frac{2K}{Cr^2\rho}t$$

by substituting the numerical values we have $t = 0.5-1$ ns and the average cooling rate is $\leqslant 10^{12}$ K s^{-1}. It is these estimates that are indicated in publications dealing with laser ablation in liquids.

Thus, performing ablation in a liquid medium, first, increases the efficiency of the process and, second, prevents destruction of ablated substances, as shown in relation to readily destroyed phosphides and organic compounds.

3. Technical implementations

The LAL technique is distinguished by simple technical implementation. A compact target is placed on the bottom on a vessel filled with a liquid. A laser beam is focused onto the liquid/target interface. Actually, this is the basic configuration of the setup.

However, depending on the task to be solved, some auxiliary systems and devices can also be used. For example, to prevent the oxidation of particles, inert gas is bubbled into the liquid and to induce oxidation, oxygen is bubbled. Magnetic stirring is used to homogenize the colloid solution of nanoparticles; alternatively, the vessel with the liquid is placed into an ultrasonic bath (Fig. 5). If

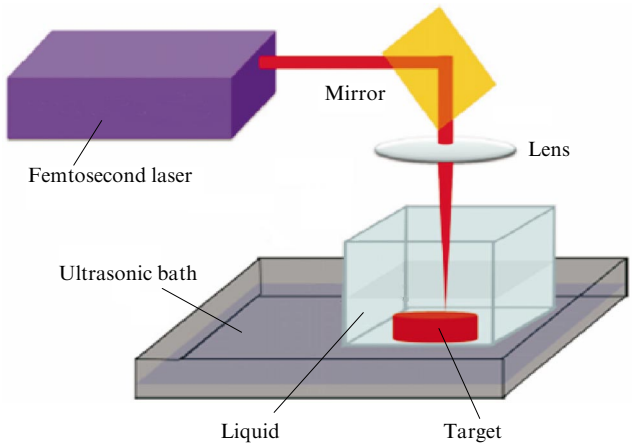


Figure 5. Schematic diagram of a typical experimental setup for LAL.[19]

repeated treatment of highly dispersed particles is required, the laser beam is directed parallel to the target surface through the colloid solution bulk. In a publication,[4] splashing of the liquid occurred as the radiation power increased. In order to avoid the undesirable consequences, the authors directed the radiation at the Brewster angle (Fig. 6) and to minimize the reflection losses, *p*-polarized radiation was used.

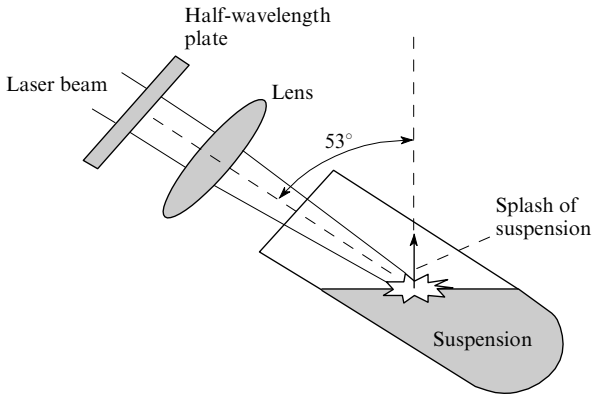


Figure 6. Geometry of irradiation of a solution.[4]

A key problem solved by LAL is preparation of a colloid solution of nanoparticles by disintegration of the appropriate compounds. From a colloid solution, dry nanoparticles can be recovered, or it can be used for the formation of films and coatings, for the subsequent synthesis in the case of insoluble compounds, and so on. In some cases, for solving problems of this type, starting materials already disintegrated in some way are used. Ruth and Young [74] considered the effect of laser treatment on the properties of CdSe and CdTe colloid solutions obtained by LAL. They used a Nd:YAG laser ($\lambda = 532$ nm, $\tau_p = 600$ ns, $E_p = 1-7$ mJ, $\rho_W = 5-30$ MW cm^{-2}).

The observed changes in the transmission spectra can be attributed, at the first glance, to agglomeration (which may be promoted by laser radiation) and precipitation of particles. However, normalization of the spectra in the visible region (Fig. 7) reveals an increase in the short-wavelength absorption, which in turn attests to a decrease in the average particle size. This effect can also be due to both predominant precipitation of large particles and particle disintegration under the action of laser radiation. After being kept for several weeks, the colloid solutions remained stable; therefore, the authors gave preference to the model of particle disintegration by laser radiation. Meanwhile, additional irradiation of a degassed colloid solution did not change considerably the transmission spectra, which rather indicate that the spectral changes occurring upon additional treatment (Fig. 8) are caused by oxidation of the substance.

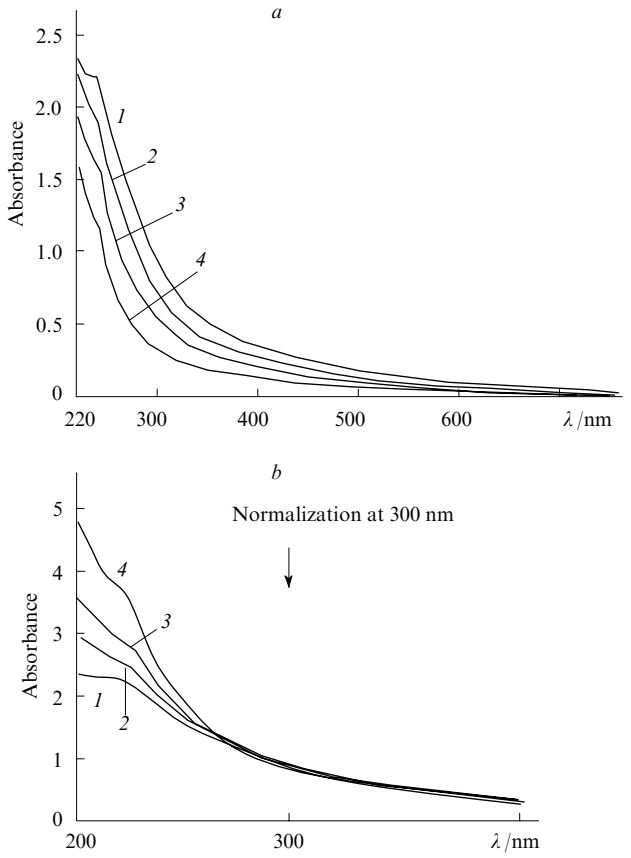


Figure 7. Non-normalized (*a*) and normalized (*b*) absorption spectra of CdSe particles in acetonitrile (*1*) and additionally treated colloid solutions (*2–4*) at a repetition frequency of 1500 Hz, a pulse energy of 1.8 mJ and the same wavelength.[74]
(*1*) CdSe particles in acetonitrile; treatment of colloid solutions for 20 (*2*), 40 (*3*) and 80 min (*4*).
All spectra were recorded at room temperature and corrected for scattering and absorption by the solvent. Figure 7 *b* shows the same spectra normalized with respect to each other at 300 nm.

Apart from the repeated irradiation of the nanoparticles prepared by LAL, in some studies, the microparticles (HfS_3,[75] Ag_2S,[76] FeO,[77] Bi_2Te_3,[78] Si [79, 80]) prepared preliminarily by other methods were subjected to laser radiation. It was noted [81, 82] that this approach increases the productivity of the method with respect to ablation of monolithic materials. Ablation of a suspension of microparticles was

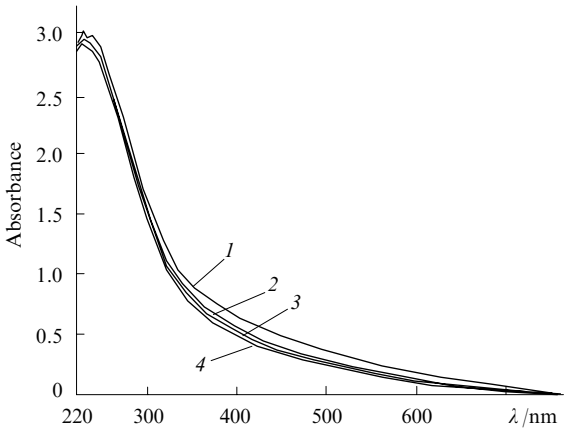


Figure 8. Absorption spectra of CdSe nanoparticles obtained by primary ablation for 15 min in degassed acetonitrile (repetition frequency 50 Hz, pulse energy 3 mJ, wavelength 532 nm) and colloid solutions of these particles that were additionally treated at repetition frequency of 1500 Hz, a pulse energy of 1.8 mJ and the same wavelength.[74]
(*1*) Initial CdSe sample, (*2*) the sample after a 30-min irradiation, (3) the sample after a 60-min irradiation, (*4*) the sample after a 120 min irradiation.
All spectra were recorded at room temperature and corrected for scattering and absorption by the solvent.

used[40] to prepare PbTe nanoparticles. The production of 4–6 nm nanoparticles (80% of the material) from the pre-dispersed compound (20–100 μm) required a five-minute irradiation by 200 mJ Nd : YAG laser pulses at $\lambda = 532$ nm and 400 mJ pulses at $\lambda = 1064$ nm. This yielded 50 mg of nanodispersed PbTe. The above attests to high performance of LAL applied to a pre-dispersed material. Note for comparison that in another study,[33] an order of magnitude longer LAL process was used for monolithic silicon (for the same amounts of substances).

It follows from the foregoing that the LAL method, which is easily technically implemented, provides a high degree of material dispersion and is suitable for the additional dispersion of materials disintegrated by other methods.

4. Ablation in liquid accompanied by chemical reactions

The LAL method was used to synthesize silver selenide nanoparticles from silver nitrate and selenium powder added to a mixture of isopropyl alcohol and ethylenediamine followed by argon purging to remove the dissolved oxygen.[1] The radiation of a neodymium laser ($\lambda = 1064$ nm, $\tau_p = 7$ ns, $\nu = 10$ Hz, $\rho_W = 10^9$ W cm^{-2}, $t = 30$ min) was used. The silver selenide thus obtained was characterized by powder X-ray diffraction, electron microscopy and X-ray photoelectron spectroscopy. The average size of spherical Ag_2Se particles was 30 nm and it increased when the reaction was performed in pure isopropyl alcohol or when the time of treatment increased from 30 to 90 min. Thus, in the study cited,[1] the LAL method actually performed the same function as microwave radiation in the synthesis of copper selenoindate in polyethylene glycol from copper chloride, indium acetate and selenium powder.[83]

Using laser ablation in oxygen-containing liquids, it is possible to form an oxide film on the surface of nanoparticles immediately after they have formed. When such film is present, the surface is passivated, the concentration of surface defects decreases, and this is beneficial for some properties, in particular, luminescence properties (the half-width of the luminescence spectral line decreases), as was shown for silicon.[33]

The ablation of InP in water was accompanied[34] by partial oxidation, and traces of indium oxide were detected (nothing was said about preliminary removal of oxygen from water). Note that ablation of various metals in water was reported to be usually accompanied by partial oxidation of the product.[84] This is also indicated by other studies: copper ablation in water gives CuO nanoparticles,[85,86] indium gives In_2O_3,[24] tin is converted to SnO_{n-2} (Ref. 87) and ablation of magnesium produces $Mg(OH)_2$.[88] The mechanism of metal oxidation during the ablation in water has been discussed.[87–89]

Meanwhile, bismuth telluride was produced by ablation in water and no signs of oxidation were detected.[81] A similar result was reported for zinc selenide and cadmium sulfide.[90] When these compounds were ablated in water, isobutyl alcohol, diethylene glycol, ethanol or dimethyl sulfoxide, nanoparticles of the same compounds were formed. The ablation in water did not result in a change in the chemical composition of CdS or As_2S_3,[30] and the structure of PbTe was retained after ablation of a suspension of its microcrystals in water for 5 min but degraded after long-term (45 min) ablation.[40]

The use of organic liquid media in some cases restores the ablated material. For example, ablation of CuO in isopropyl alcohol induces a process opposite to the process involved in the copper ablation in water (see above), particularly, copper nanoparticles are formed.[91] Tsuji *et al.*[20] ablated cobalt and cobalt oxides (CoO, Co_2O_3) in water and hexane using the third harmonic radiation from a Nd : YAG laser ($\lambda = 355$ nm, $E_p = 30$ mJ). It was found that in water, all three starting materials produce cobalt sesquioxide nanoparticles, while in hexane, the ablation of cobalt and Co_2O_3 affords cobalt nanoparticles, and the ablation of CoO gives mainly CoO nanoparticles.

By ablation in water, nanoparticles of $Sr_2MgSi_2O_7 : Eu^{2+}, Dy^{3+}$, which is a luminophore with a long luminescence relaxation time, were reported.[18] The researchers found that in addition to the nanoparticles having the same composition and structure as the target, the $SrCO_3$ particles were formed as a by-product when the target material reacted with carbon dioxide dissolved in water. As expected, the amount of the by-product increased with increase in the laser radiation fluence (Fig. 9). The third harmonic of a Nd : YAG laser was used ($\lambda = 355$ nm, $\tau_p = 50$ ns, $E_p = 0.5$ mJ, $\nu = 4$ kHz).

Magnesium ablation has been carried out in various solvents.[92] The first harmonic radiation from a Nd : YAG laser was used ($\lambda = 1064$ nm, $\tau_p = 5.5$ ns, $E_p = 75$ mJ, $\nu = 10$ Hz). This pulse energy corresponds to fluence of 0.27 or 33 kJ cm^{-2} at the focal point. The treatment time was 60 min. The ablation in acetone or isopropyl alcohol yielded MgO and Mg nanocrystals, while in deionized water or in aqueous sodium dodecyl sulfate, $Mg(OH)_2$ nanocrystals formed. It is noteworthy that the chemical composition and the structures of the ablation products formed in deionized water and in sodium dodecyl sulfate dissolved in water (0.08 mol litre^{-1}) coincide; however, their morphologies are drastically different (Fig. 10).

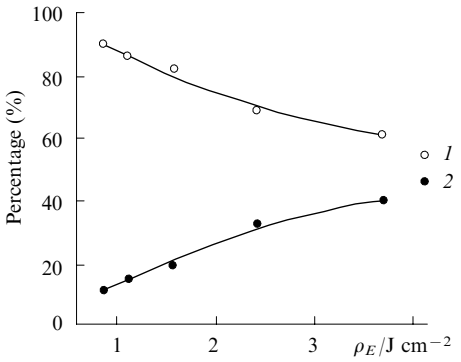


Figure 9. Percentages of the luminophore $Sr_2MgSi_2O_7:Eu^{2+},Dy^{3+}$ (*1*) and the by-product $SrCO_3$ (*2*) in ablated material *vs.* radiation fluence.[18]

The possibilities of LAL as a tool for controlled and targeted chemical synthesis were demonstrated[28] in relation to the preparation of the double layered hydroxide $Mg_6Al_2(OH)_{18}\cdot 4.5(H_2O)$. The first harmonic radiation from a Nd:YAG laser was used ($\lambda = 1064$ nm, $E_p = 75$ mJ, $\nu = 10$ Hz). The time of magnesium ablation in deionized water varied from 5 to 60 min. The aluminium ablation time was invariably 30 min. The first stage was the ablation of magnesium to give $Mg(OH)_2$, while the second stage was aluminium ablation to give $Al(OH)_3$ followed by the formation of the double layered hydroxide. By varying the duration of magnesium ablation, one can change the concentration ratio of aluminium and magnesium hydroxides in the solution. When the magnesium ablation lasts for <25 min or >35 min, the excesses of aluminium hydroxide and magnesium hydroxide, respectively, form separate phases in addition to the double hydroxide phase, and the interlayer spacing in the double hydroxide structure changes only slightly (Fig. 11). When the ablation of magnesium lasts for 25–35 min, only double hydroxide structures are formed with variable magnesium to aluminium ratio in the positively charged layers. As the content of the doubly charged (magnesium) ions increases, the electrostatic attraction between the layers diminishes and the interlayer spacing grows. Thus, using the LAL method, it is possible to control the composition of the phase being synthesized within the homogeneity region.

It was noted[30] that low stability of the colloid solutions obtained by the LAL method is the 'cost' of the convenience of application of this method, and it was proposed to use more viscous media. For example, a colloid solution in ethanol obtained by LAL can be dissolved in oil and the ethanol can be evaporated.

The ablation of silicon in a liquid solution of ethyl polysilicate in an ethanol – ethyl acetate mixture was reported.[33] Just after the ablation, the colloid solution was sonicated and heated for polymerization (curing) at ~ 50 °C for 24 h. The presence of the silicon-dioxide-based polymer in the liquid medium promotes passivation of the nanoparticle surface as a result of formation of the oxide film; this treatment gives rise to blue luminescence. For surface passivation and appearance of blue luminescence in an aqueous colloid solution, it had to be stored for several weeks.[93]

Thus, the LAL method can be utilized for conducting chemical reactions. By varying the conditions of the laser ablation in liquid, one can adjust the process to be accom-

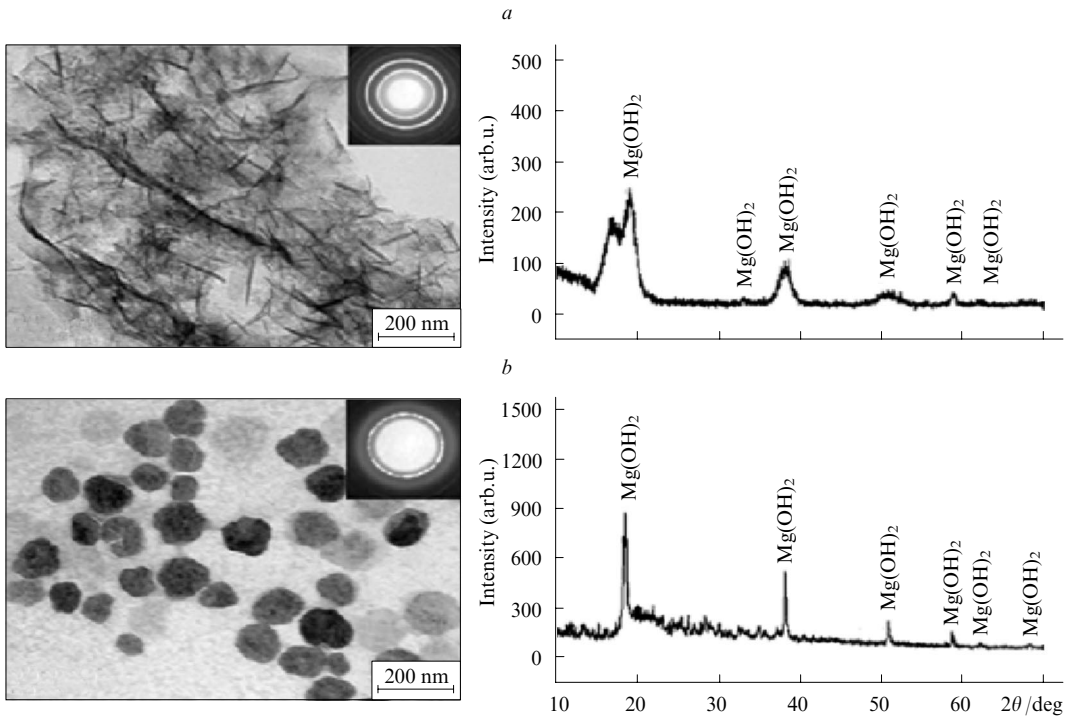


Figure 10. TEM images (on the left) and X-ray diffraction patterns (on the right) of the products of magnesium ablation in deionized water (*a*) and in a 0.08 M solution of sodium dodecyl sulfate (*b*).[92]

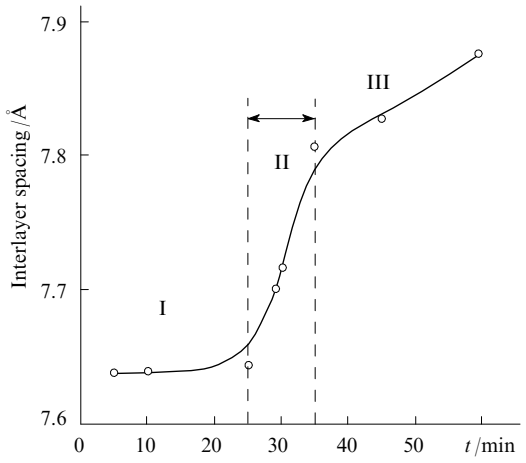


Figure 11. Interlayer spacing in $Mg_6Al_2(OH)_{18} \cdot 4.5\,H_2O$ *vs.* magnesium ablation time (for ablation conditions, see the text).[28]
I and III are multiphases, II is a single phase.

panied by both partial (or complete) oxidation of products to give oxides or chalcogenides and reverse process, *i.e.*, the reduction of the ablated oxides. Moreover, nanoparticles of complex oxides with controlled stoichiometry can be obtained.

5. Effect of the medium on laser ablation in liquid

A liquid medium can either accelerate[94] or substantially decelerate[95] sedimentation. The stability of an aqueous colloidal silver solution decreases upon the addition of NaCl.[96] Upon increase in the sodium dodecyl sulfate concentration, the average particle size of silver decreases and the colloid solution becomes more stable.[95] In a study of the effect of water, toluene, ethanol and xylene on the CdS and As_2S_3 nanoparticle size,[30] the following conclusions were made taking into account the position and the slope angle of the fundamental absorption edge of colloid solutions. In all cases, except for xylene, the nanoparticle size and suspension stability did not depend on the solvent. When xylene was used, coarser particles with a narrow size distribution formed and the colloid solution was more stable with respect to sedimentation. However, the shift of the fundamental absorption edge of the colloid solution observed in xylene was rather attributed to solvatochromic effect and not to increase in the particle size. Taking account of this effect, the particle sizes were estimated as follows: 1.5–2.3 nm for CdS and 1.5–3 nm for As_2S_3. As regards the narrower particle size distribution and the colloid solution stability, these were attributed to higher xylene viscosity compared to other solvents used in the work. This attests to advantages that can be gained by using high-viscosity organic solvents. For example, it was noted[97] that a narrower CdS particle size distribution is obtained in polyvinylpyrrolidone (PVP) than in water. In another publication,[98] PVP was used to stabilize a colloid solution of metallic particles exhibiting nonlinear optical properties.

Most liquids have a negative sign of the thermal optical nonlinearity of the refractive index, resulting in beam self-defocusing upon laser ablation. In this respect, water is a specific medium for laser ablation,[74] as its heat capacity and heat conductivity are ~2 and ~3 times, respectively, higher than those of other liquids used and the temperature factor of the refractive index is 4–5 times lower. This was invoked to explain the difference between the transmission spectrum of a CdSe colloidal solution prepared by LAL in water and the spectra of CdSe solutions obtained in other media (Fig. 12). Laser pulses of 600 ns duration were used for which the thermal optical effects are significant.

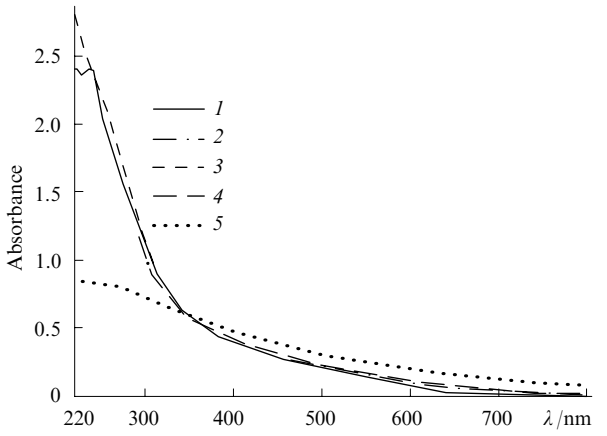


Figure 12. Absorption spectra of suspended CdSe nanoparticles obtained by ablation in different solvents.
Solvent: (*1*) acetonitrile, (*2*) acetone, (*3*) butan-2-ol, (*4*) ethanol, (*5*) water.[74]
All spectra were normalized at 350 nm. In all cases, ν = 50 Hz, E_p (mJ) and t (min), respectively: for acetonitrile, 3.5 and 3; for acetone, 1.0 and 30; for butan-2-ol, 7.0 and 30; for ethanol, 1.5 and 60; and for water, 3.0 and 60 (off-focus).

However, it was pointed out[32] that the luminescence properties of CdS and GaAs colloidal solutions rapidly degrade in water, while in ethanol, they are preserved for at least a year.

A colloid solution of perylene-3,4,9,10-tetracarboxylic acid dianhydride nanoparticles was prepared by LAL.[48] The researchers used a suspension of microparticles and third harmonic radiation from a Nd : YAG laser. The nanoparticles were formed only in polar solvents (water or ethanol), while in non-polar solvents (cyclohexane and toluene), no nanoparticles could be obtained. The authors explained this by assuming that polar solvents prevent the nanoparticles from aggregation.

Thus, the nature of the liquid medium considerably affects the outcome of laser ablation. When choosing the liquid medium, one should consider not only its chemical properties but also the rheological, optical (including nonlinear optical), thermal, dielectric and some other properties.

6. Effect of laser treatment parameters on the ablation in liquid

The choice of the laser radiation wavelength was discussed in a number of works (see, for example, Ref. 30). The following has to be taken into account. On the one hand, radiation should be absorbed by the ablated substance, and this is determined by the position of the fundamental absorption edge. Simultaneously, the ablated nanoparticles would also absorb radiation and decrease the process efficiency (the methods for partial removal of the nano-

particles from the ablation zone fail to solve this problem completely). The position of the fundamental absorption edge depends on the particle size if it is smaller than the exciton Bohr radius (R_B). The parameter R_B is mainly determined by the substance nature. For CdS, CdSe, Ge and PbS, it is 3.05, 4.9, 24.3 and 18 nm, respectively. The nanoparticle size, in turn, depends on the wavelength of the radiation used. For example, a study of the LAL of silver (λ = 355, 532 and 1064 nm) showed[29] that at λ = 355 nm, the laser ablation is most efficient and the particle size distribution is much narrower than at λ = 1064 nm. According to Singh *et al.*,[22] the third harmonic wavelength of a Nd : YAG laser was also chosen as most efficient in the ablation of Gd_2O_3-based ceramics doped by erbium and ytterbium, which is caused by the strong enhancement of the radiation absorption by the colloid solution on going to the first harmonic. By the efficiency of ablation is meant the process productivity. In the same publication, the optimal radiation intensity was 81 J cm^{-2}; at this intensity, completely spherical nanoparticles were formed.

Using a Nd : YAG laser in the Q-factor modulation mode (ν = 10 Hz, τ_p = 5 ns, E_p = 12 mJ), InP nanoparticles were obtained.[65] As a result of focusing, the fluence was 3.5 J cm^{-2}. Ethanol was used as the liquid medium. Fourth harmonic radiation (λ = 266 nm) gave rise to 2–3 nm non-crystalline particles, while second harmonic radiation (λ = 532 nm) resulted in 4–10 nm particles with a well-formed crystal structure (Fig. 13). The ratio of phosphorus and indium contents was 2 : 5 when long-wavelength radiation was used and 1.21 : 1 in the case of short-wavelength radiation. The observed effect of the radiation wavelength on the properties of the products of indium phosphide ablation in ethanol was reasonably attributed to the fact that the penetration depth of the short-wavelength radiation is 9 nm and that for the long-wavelength radiation is 105 nm. Hence, in the former case, much faster heating and (what is more important) cooling of the material take place, and these processes give rise to sharp temperature gradients. A smaller amount of substance is heated to a higher temperature. According to estimates, the cooling rate was 1.45×10^{18} K s^{-1} in the former case and 1.1×10^{15} K s^{-1}, *i.e.*, three orders of magnitude lower, in the latter case.

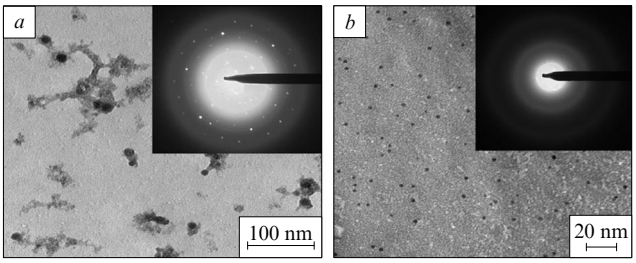


Figure 13. Electron microscope images of InP particles obtained by ablation in ethanol at λ = 532 (*a*) and 266 nm (*b*).[65]
It can be seen in the X-ray diffraction patterns in the inserts that at λ = 266 nm, the particles are amorphous.

Chubilleau *et al.*[40] considered the effects of the wavelength of a Nd : YAG laser, the duration of treatment and the power of radiation on the ablation of PbTe pre-dispersed in water (20–100 μm). The nanoparticle size, morphology and the formation efficiency were analyzed. Three laser radiation wavelengths were used, 1064, 532 and 266 nm; the pulse energy was varied from 120 to 400 mJ, which corresponds to a fluence of ~15–60 J cm^{-2} at the focus and 7–28 J cm^{-2} on the solution surface. During the treatment time of 1–5 min, the number of pulses was 600–3000. The highest energy of laser pulses is 120, 530 and 1100 mJ for λ = 266, 532 and 1064 nm, respectively; however, in experiments, it was restricted by the value of 400 mJ in order to avoid the substance splashing. The λ = 266 nm radiation was found to be relatively ineffective. When irradiation was done by pulses at λ = 532 and 1064 nm and E_p = 200–400 mJ, even after the first minute of treatment, 67% of the particles were already 3–7 nm in size and 30% were 7–30 nm in size. After five-minute treatment, 80% of particles had a size of 4–6 nm and no particles larger than 20 nm were present.

Thus, longer treatment produced more monodisperse particles. However, further increase in the treatment time (up to 45 min) induced destruction of the compound, as was indicated by X-ray diffraction patterns. Note that an increase in the pulse energy from 200 to 400 mJ did not lead to the expected decrease in the particle size. Analogous results were obtained in another study.[99] Presumably[40] (see also Ref. 99), in lead telluride ablation, increase in the pulse energy results in warming-up, melting and, consequently, in the aggregation of particles surrounding the particle that has absorbed the photon. Thus, dispersion and aggregation counterbalance each other. It was noted that the particle size distributions after five-minute treatments at λ = 532 nm, E_p = 200 mJ and at λ = 1064 nm, E_p = 400 mJ are similar. However, the conditions of choice for dispersion are λ = 1064 nm, E_p = 400 mJ and t = 5 min.

Indium sesquioxide was prepared by ablation of indium in water.[24] The researchers suppose that increase in the laser radiation intensity does not promote the formation of more dispersed particles but the reasoning they give is different. There are two key ablation mechanisms under the action of a laser pulse: vaporization and microexplosion. The former mechanism prevails at low radiation intensity. In a space confined by a dense liquid medium with rather fast heat withdrawal, phase nuclei are formed, rapidly grow and then coalesce. The nanoparticle formation rate and nanoparticle size are determined by the temperature and concentration of the ablated substance. Larger particles (tens of nanometres in size) are formed if the explosive ablation mechanism predominates, while if vaporization prevails, more dispersed particles (several nanometres in size) are formed. As applied to the experimental conditions they used for ablation of indium in water by means of second harmonic radiation from a Nd : YAG laser (λ = 532 nm, τ_p = 5 ns, ρ_E = 0.5–10 J cm^{-2}), the researchers cited proposed[24] that vaporization was the predominant mechanism and, therefore, the average particle size was < 10 nm.

Nanoparticles of the luminophore $Sr_2MgSi_2O_7 : Eu^{2+}$, Dy^{3+} with long luminescence relaxation time were produced by ablation in water.[18] It was confirmed experimentally that an increase in the radiation fluence leads to particle coarsening (Fig. 14). The third harmonic of a Nd : YAG laser was used (λ = 355 nm, τ_p = 50 ns, E_p = 0.5 mJ, ν = 4 kHz).

The effect of pulse duration on the results of LAL is also miltifactorial.[30] Nanosecond radiation is considerably

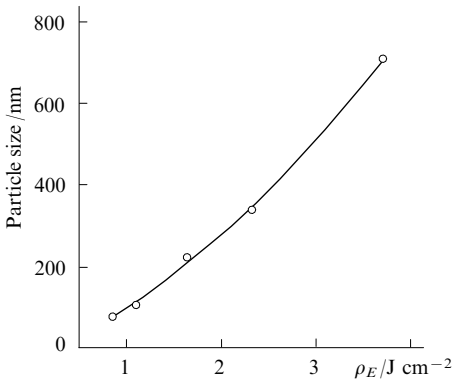


Figure 14. Average particle size of the luminophore $Sr_2MgSi_2O_7:Eu^{2+},Dy^{3+}$ *vs.* laser radiation fluence.[18]

affected by thermal effects caused by linear absorption. For shorter pulses, the multiple photon absorption and the optical Kerr nonlinearity make their contributions. For most of liquids, the sign of the thermal optical nonlinearity of the refractive index is negative. This results in beam self-defocusing, and, as shown, for example, in Ref. 29, the focal point should be located 5 mm ahead of the target.

The use of femtosecond pulses allows for achieving higher temperatures and pressures and for producing more dispersed particles with a narrow size distribution.[58,100] Perhaps, it is the high temperature developed during the femtosecond ablation of bismuth oxide in ethanol that is responsible for its disproportionation with a 15% decrease in the oxygen content with the crystal structure being retained.[19] Also, it should be borne in mind that bismuth is located in the same row as chalcogens and its oxide has moderate stability.

The role of the pulse duration was clearly demonstrated by Dolgaev *et al.*,[101] who ablated sapphire in aqueous solutions. They considered this process to be largely determined by the attainment of high temperature and pressure, which induce water transition to the supercritical state. Evidently, this is impossible for long pulses (150 μs), and, as it is shown, no sapphire ablation takes place.

Tsuji *et al.*[4] carried out ablation of $LiMn_2O_4$ microparticles in aqueous medium using the fundamental harmonic of the Nd:YAG laser (λ = 1064 nm, τ_p = 6 ns, E_p = 30 and 150 mJ). It was found that increase in the pulse energy substantially accelerates the process, while the particle size is thus decreased.

An interesting scheme for investigation of the effect of laser radiation intensity was implemented [102] in the production of zinc oxides by ablation of zinc metal in deionized water. The ablation was performed in three modes in particular, the water–zinc interface was located above the focal plane (I), in the focal plane (II) or below the focal plane (III). The results of experiments are given in Fig. 15 and in Table 1.

The considerably lower fluence (and the proper pulse energy) for a position of the target below the focal plane compared with the position above the focal plane is associated with the energy loss for plasma formation at the focal point in water.

Thus, the influence of laser radiation parameters (wavelength, pulse duration and power, treatment time) is rather

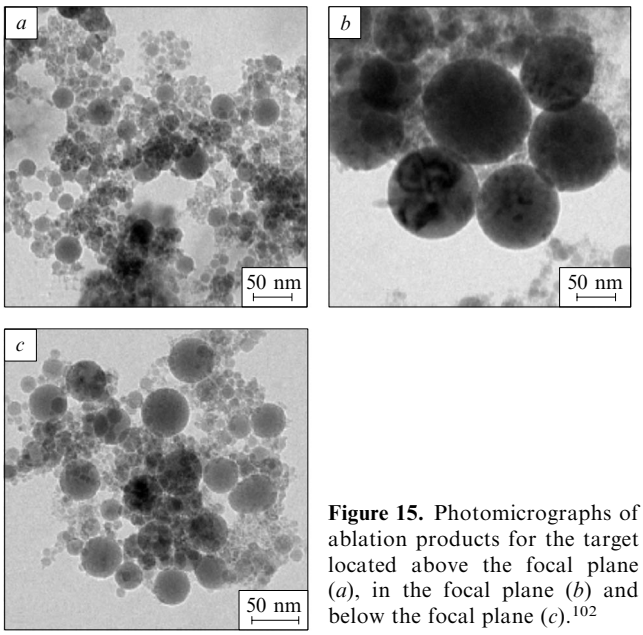


Figure 15. Photomicrographs of ablation products for the target located above the focal plane (*a*), in the focal plane (*b*) and below the focal plane (*c*).[102]

Table 1. Effect of laser fluence on the composition and structure of the ablation products.

Target position	ρ_E /J cm^{-2}	Average particle size /nm	Particle size scatter /nm	Phases present
I	1.4	12	2–45	$TiO_{1.5}$
II	80	13	4–205	TiO_2 (rutile), $TiO_{1.5}$
III	0.2	9	3–75	TiO_2 (anatase), $TiO_{1.5}$, Ti

intricate, which can be used to adjust the ablation conditions for a particular task. In most cases, for preparing monodisperse particles, it is desirable to use short pulses of short-wavelength radiation of limited power.

Generally, it should be noted that LAL is a technically simple method suitable for the preparation of diverse materials in the nanodispersed state. An advantage of the method is that the nanodispersed substance occurs in a colloid solution and the particle size can be brought to several nanometres. Therefore, this method is very efficient for research. It is suitable for preparing a relatively small amount of nanodispersed substance, which is quite sufficient for scientific research.

III. Laser ablation in vacuum: thin film deposition

Currently laser ablation is considered to be an efficient and flexible technique for the manufacture of thin-film micro- and nanostructured materials. A procedure based on the laser ablation phenomenon can be employed to produce high-quality amorphous and crystalline, dielectric, semiconducting and conducting, mono- and multilayer, single- and multicomponent thin films for solving a broad range of tasks, in particular, in classical integrated optics, medicine, electronics, *etc.*

The LAV process followed by deposition of the ablated substance on a substrate underlies the method of pulsed laser deposition (PLD) of thin films. The film deposition

occurs in a vacuum chamber or in a reactive or buffer gas atmosphere. The properties and the quality of produced films depend on the deposition conditions, particularly, on laser radiation parameters, vacuum chamber conditions, composition of the target (elements or compounds) and the substrate (amorphous or crystalline material), their temperature, rotation rate, *etc*. Note that the formation of laser plasma and specific features of its expansion and deposition onto the substrate are determined by extremely intricate and multifactorial physical processes dependent on the whole set of experimental parameters. Detailed description of the plasma formation, expansion and condensation processes that develop upon laser ablation is beyond the scope of this review as it is comprehensively dealt with in a number of monographs.[103–105] The key parameters of PLD are described below and their influence on the chemical composition, morphology and structure of the films being formed is demonstrated.

The possibility of varying PLD conditions over a broad range and the diversity of materials suitable as targets are the factors responsible for the unique functional properties of the thin-film structures that are formed. The PLD method can be used to produce oxide, nitride, carbon-containing, metallic, polymeric, *etc*. films with specified contents of components; more than 200 sorts of films prepared by this method were reported.[106, 107]

The undoubted benefits of PLD over other methods of thin-film manufacture include the relative simplicity of experimental implementation, minor engineering modification of the setup for deposition of films of various types and compositions, the possibility of using hybrid processes (additional physical treatment — heating, irradiation, *etc*.), flexible deposition conditions and fast system response to the change in the treatment conditions. An important advantage of the method is the possibility of material transfer from the surface of a target with complex composition to the substrate without change in the chemical composition, which is a consequence of the non-equilibrium nature of laser ablation.[107]

The PLD method is used to produce thin films, which are demanded in nearly any field of modern science and technology — for the manufacture of transparent conducting oxide films, polymeric films, high-temperature superconducting films, thermoelectric, piezoelectric and ferroelectric materials for electronic systems, various sensors, medical drug delivery systems, *etc*. An important application is the design of active and passive thin-film optical components for the modern optical informatics.[107] As a rule, these optical components are based on amorphous or crystalline thin films with desired linear/nonlinear response coefficients and with minimized optical loss and minimized number of defects.

1. Experimental implementation of pulsed laser deposition

a. Setup diagram

The basic configuration of the setup for pulsed laser deposition of thin films is shown in Fig. 16. The film is formed in the deposition chamber either in a high vacuum or in the gas atmosphere of the specified composition. The laser radiation is focused on the target surface at a 45° angle through an optical window of the chamber. The formation of a steady plume of the ablated substance is provided by either laser beam scanning of the target surface (in this case, the target surface area should be rather large, at least

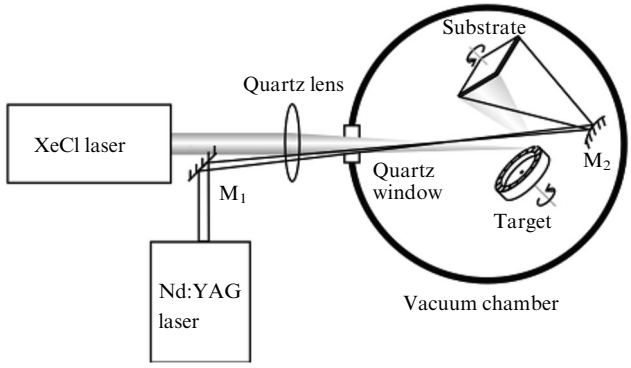


Figure 16. Optical scheme of the PLD complex.
M_1, M_2 are interference mirrors; Nd : YAG laser is used for optical heating of the substrate.

1 cm^2)[108] or by using a rotating target, in particular, a target composed of many samples.[109] In the latter case, samples of different compositions can be combined in the target, and, hence, thin films of specific chemical composition with unique properties can be obtained. In addition, the use of a composite target comprising several samples, it is possible to create multilayer thin-film structures with individual compositions and structures of each layer.[110]

The substrate onto which the film is deposited is, most often, located parallel to the target surface at a 2–10 cm distance from the target. In some cases, for obtaining the desired chemical composition and structure of the film being formed, the substrate is to be heated. A specific feature of the scheme presented in Fig. 16 is the possibility of thin film deposition onto the substrate using laser heating. The major advantage of the optical heating is the lack of mechanical contact between the heater element and the substrate, which makes substrate rotation much easier. The laser radiation source for substrate heating is chosen taking into account the optical properties of the substrate to ensure effective absorption of the optical radiation and, hence, effective heating.

b. Laser sources

In the PLD of thin films a pulse laser serves as the energy source for target vaporization and atomization, the laser wavelength being chosen taking into account the optical absorption of the target to ensure the sufficient absorption of pulse energy and effective ablation of the substance. As a rule, most of materials have high absorption coefficients in the UV range; therefore, lasers that generate UV radiation, first of all, excimer lasers are preferred for film PLD.

Laser	ArF	KrCl	KrF	XeCl	XeF
λ/nm	193	222	248	308	351

Currently, excimer lasers successfully compete with Nd : YAG lasers, as they have higher UV photon energy without the use of high harmonics.[111]

The first experiments on pulsed laser deposition and formation of thin films on semiconducting, dielectric, chalcogenide and organometallic substrates were carried out by Smith and Turner[112] using a ruby laser. Later, the possibility of using a neodymium glass laser[113] and a CO_2 laser[114, 115] was demonstrated. The development of laser

technology made it possible to pass from millisecond pulses and the quasi-steady-state ablation mode where the material is ablated mainly due to thermal processes to ultrashort, pico- and femtosecond laser pulses, and to development of non-equilibrium processes determined by photophysical ablation mechanisms and resulting in stoichiometric transfer of the material from the target to the substrate.[116, 117]

It is noteworthy that the intensity of laser radiation and pulse duration are the key laser parameters that determine not only the ablation mechanism, the properties of the ablated substance flux, the substance ionization degree, the energy and velocity of ablated species but also (as a result) parameters of the deposited film. From the standpoint of PLD process efficiency, these parameters are considered to be optimized if a monomolecular layer is deposited per pulse. When producing thin films with desired functional properties, which are mainly determined by the chemical composition and the structure of the deposited substance, particular attention should be devoted to optimization of the above-listed key laser radiation parameters.

c. Effect of the laser radiation pulse duration

The pulsed laser deposition procedure for the formation of film structures is based on the non-equilibrium nature of the laser ablation process caused by the impact on the target of short laser pulses with high peak intensity. In most cases, the laser-induced vaporization from the target surface is governed by the heat diffusion length, which is proportional to $\sqrt{\tau_p}$. It is believed that for >20 ps pulses, the laser ablation occurs due to thermal processes.[118, 119] In the case of shorter pulses, the optical impact time is shorter than the characteristic time of transformation of the absorbed energy to heat. From the physical standpoint, this means that only photoexcitation and fast electronic processes (including electron emission) develop during the pulse impact time, and this results in efficient ablation of the substance.

Thus, the physics of laser ablation processes developing under the action of pulsed radiation is mainly determined by laser pulse duration, which considerably affects the properties of the films being formed. The plasma images taken 10 ns after the impact of femto- and nanosecond laser pulses on the silicon surface are presented in Fig. 17.

According to calculations based on experimental data, the shock wave front propagation velocities measured 5 ns after the pulse were 13.6×10^5 and 7.9×10^5 cm s^{-1} for femto- and nanosecond laser treatment, respectively. In addition, note the strong effect of the laser pulse duration on the pattern of plasma propagation: in the case of femtosecond pulses, the velocity of plasma propagation in the direction normal to the target is much higher than the propagation velocity in the transverse direction (parallel to the target); in the case of nanosecond laser pulses, the plasma propagation velocity is nearly the same in any direction.

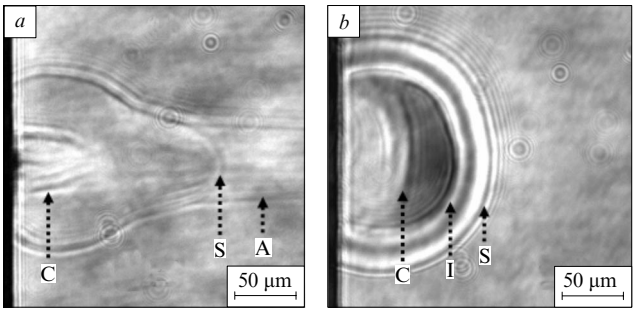


Figure 17. Plasma images obtained 10 ns after the action of femto- (*a*) and nanosecond (*b*) laser pulses on a silicon surface.[120]
C is the contact front between the ionized target material and the ionized atmosphere, I is the ionization front, S is the shock wave front, A is gas discharge plasma.

Studies of the effect of laser pulse duration on the PLD processes demonstrated that pulses of about 10 ns (or longer) have adverse influence on the morphology and the properties of the target, because the target surface is destroyed (caverns and microcracks are formed) and the composition changes as a result of chemical reactions. The change in the target properties deteriorates the properties of deposited films due to the increase in the numbers of drops and clusters in the flux of ablated substance and disruption of the chemical composition. Decrease in the pulse duration, in particular, transition to subpicosecond pulses, minimizes the structural damages of the target and improves the properties of the films.[121–123]

The use of femtosecond laser pulses substantially (by 1–2 orders of magnitude) reduces the laser ablation threshold and brings the process efficiency closer to 100%. In this case, the laser radiation energy is spent almost completely for substance ionization and ablation, and the thermal effects determining the presence of microdrops in the ablated substance flux are minimized.[119] Yet another important feature of the use of ultrashort laser pulses is the possibility of very precise control over the amount of ablated substance (and, hence, the film deposition rate), which is a key parameter determining the functional properties of films. For example, it was shown [122] that for the use of 34 ns and 450 or 50 fs laser pulses (for fluences of 4, 4 and 0.4 J cm^{-2}), the AlN film deposition rate decreased from 0.7 to 0.01 and 0.0033 Å per pulse.

d. Effect of laser radiation energy

The energy parameters of the laser radiation used to initiate the ablation in the PLD method are very significant, as they influence the mechanism of substance removal from the target and the properties of the films being deposited. When the laser radiation power is low or/and the optical absorption coefficient of the material is low, local heating of the target surface most often takes place followed by the vaporization of the substance or its components (when the target is multicomponent), which obeys the thermodynamic laws of vaporization at the interface. On further increase in the energy of laser pulses as the laser ablation threshold is reached, plasma is formed, the velocity of its particles being dependent on the radiation parameters.

Numerous experiments dealing with the effect of the laser fluence on the composition, structure and morphology of films demonstrated that there is a rather narrow range of particle energies (from ~ 10 to ~ 40 eV) that is suitable for manufacturing films with desired quality and properties.[124] When the particle energy is <10 eV, the layer-by-layer film growth is inefficient, while for energies of >40 eV, noticeable particle diffusion takes place, resulting in the penetration of atoms of the film into the substrate structure and formation of defects.

When crystalline films are manufactured by PLD, the type of crystalline phase being formed also depends on the

laser pulse energy. As a rule, when the pulse energy is relatively low, the crystal structure of the film is feebly pronounced; as the radiation power increases, the resulting films have clear-cut (predominant) crystalline phase; upon further increase in energy, polycrystalline structures are formed.[125–127] In certain cases, the change in the energy parameters of the laser radiation induces a change in the type of the crystal phase formed.[128]

It is believed that this pronounced influence of the laser radiation power on the film structure is related to the kinetic energy of the ablated species. This energy should be sufficient for the atoms that reach the substrate to be able to migrate over the substrate surface and to occupy energetically favourable positions for the formation of a particular crystalline phase.[119, 126]

The use of laser radiation with high fluence (>5 J cm^{-2}) provides high rates of ablation (~ 0.01 nm per pulse). The kinetic energy of the ablated species is high and can reach 100 eV, which provides conditions for the deposition of nanocrystalline and amorphous films with unique structure and chemical composition. Most often, such films are metastable.[108, 129–131] The formation of films of this type is possible due to efficient mixing of components of the ablated substance being deposited on the substrate and insertion of high-energy plasma particles into the substrate structure or into the surface layer of the already deposited film. Usually films deposited at high laser intensities have high adhesion to the substrate.[108] The negative effects associated with film deposition under the high-power laser radiation include resputtering of the substance from the film surface back to the chamber and, as a consequence, decrease in the deposition rate. In the deposition of multicomponent films, the resputtering from the substrate to the chamber can also distort the chemical composition of the films due to different efficiencies of resputtering of various elements.[124, 132–134]

e. Atmosphere in the deposition chamber

The introduction of a buffer gas into the chamber is the most effective way to minimize the resputtering. The interaction of ablated substance species with the gas reduces the energy of plasma particles. This eliminates the resputtering effect and, despite the decrease in the number of species that hit the substrate surface, the film deposition rate increases. The decrease in the number of species that hit the substrate is caused mainly by scattering of high-energy species on the atoms of the gas; slower species of the ablated substance reach the substrate surface.[108, 135]

When the buffer gas pressure in the ablated substance flux is high, the shock wave front is formed (Fig. 18); this affects considerably the pattern of propagation of the ablated substance flux, which expands in the wave front, the velocity of plasma particles in it being further decreased.

Thus, when a buffer gas is used to reduce the expansion of plasma particles and to reach the maximum possible film deposition rate, optimization of the gas pressure in the deposition chamber is required. For example, it was shown[136] that for attaining high deposition rates of permalloy and silver films, helium at pressure 0.4 mbar, should be used.

It follows from the data presented above that the quality and chemical composition of PLD-formed films are substantially affected by the conditions in the deposition chamber, namely, the operating pressure and gas-phase composition. The nucleation rate in the ablated flux and, as a consequence, the morphology and roughness of the coating depend first of all on the pressure.[119, 137] The operating pressure also affects the stoichiometry of the film being formed; in addition, as noted above, resputtering of the material from the substrate back into the chamber becomes possible at some laser radiation parameters and pressures.

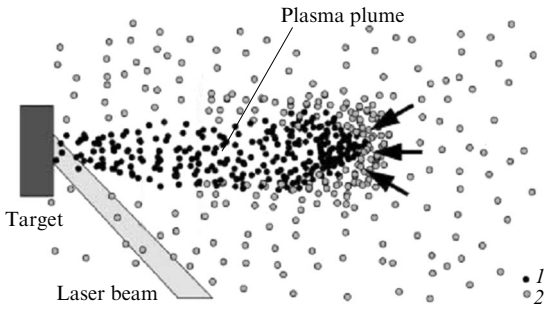


Figure 18. Model of ablation of a target in the presence of a buffer gas.[136]
(*1*) Ablated species, (*2*) gas atoms. The arrows show the area of formation of the shock wave front.

Depending on the desired chemical composition of films formed by PLD, either high vacuum or gas atmosphere of a specified composition is used. For preparing films that have the same chemical composition as the target, it is necessary to provide conditions under which the vaporized material species can hit the substrate without collisions with residual gas molecules in the vacuum chamber. Thus, films almost devoid of impurity inclusions can be obtained. As a rule, in this case, the pressure in the vacuum chamber is $\sim 10^{-9}$ mbar.[108]

For deposition of films of specific chemical composition, the presence of reactive gases in the chamber is required. For instance, oxygen or nitrogen should necessarily be present for deposition of oxide or nitride films.[138–140] In most cases of processes carried out in reactive gas atmosphere, elements, usually metals (Ti, Zn, Cu, In, ...) serve as targets. By using high-purity reactants and a definite gas atmosphere, high-quality films of specified composition can be produced.

When it is necessary to deposit films with chemical composition differing from the composition of the initial target (using compounds as the target materials), a buffer gas such as Ar, Ne, Xe and He can be used.[136, 141] The presence of the buffer gas affects considerably the expansion dynamics of the ablated material, free path lengths and collision kinetics of atoms and ions, and this ultimately determines the chemical composition of the deposited films. In addition, the buffer gas promotes nucleation in the plasma plume and deposition of nano- or microstructured films with unusual physical properties.[142]

The PLD can also be implemented with an atmosphere of complex composition (combination of gases), for example, buffer argon and reactive oxygen or nitrogen.[139, 143–145] In this case, the conditions in the deposition chamber can be varied over an extremely broad range by varying the overall gas pressure in the chamber and/or the relative contents of gases. By controlling the reactive gas pressure, which

governs the chemical reactions of this gas with the ablated species, one can control the chemical composition of the deposited films with high accuracy, while by varying the pressure of the buffer gas, it is possible to affect their morphology and, if necessary, obtain structured films.[146] Note that the use of only reactive gas at a definite (rather high) pressure for PLD can also induce nucleation in the ablated flux and the formation of structured films.

An important feature of PLD in a gas atmosphere is enhancement of the inhomogeneity of the morphology of deposited films due to the non-uniform distribution of nanoparticles and clusters in the plasma plume. The reactions of ablated species (atoms, ions, small clusters) with the gas in the deposition chamber result in scattering of light particles and focusing of heavy particles in the flux of the ablated material.[116, 147] This effect is more pronounced when a reactive gas phase is used, because during plasma expansion, chemical reactions take place, resulting in the formation of more complex (coarse) structural fragments and compounds. The quality and uniformity of the films can be attained by altering the deposition geometry.

When it is required to form films in a definite gas phase, a modified approach can be used; in particular, a portion of the reactive gas is introduced into the deposition chamber (in the direct vicinity of the target) at the instant of laser pulse arrival.[124, 148] Synchronizing the laser and gas pulses ensures the effective reaction between the ablated substance and the gas under conditions far from chemical equilibrium and the desired composition of the film can thus be obtained.[124, 149] In addition, the introduction of the gas portion strongly affects the collisions and the substance ablation dynamics (Fig. 19); owing to fast expansion of the introduced gas and considerable increase in the distance between the particles, no clusters or coarse fragments are formed in the plume.[119, 124]

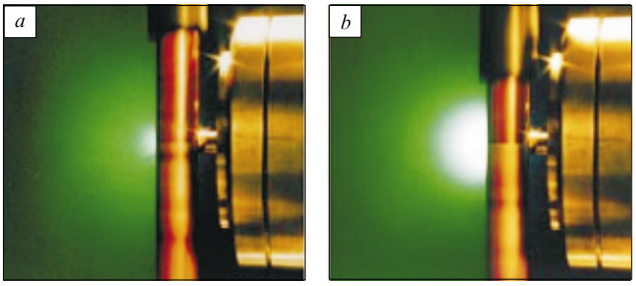


Figure 19. Ablation of a copper target in vacuum (*a*) and when reacted with introduced nitrogen dioxide (*b*).[119]

f. Methods for increasing the quality of deposited films

The principal drawbacks of PLD in the production of thin-film structures is the presence (or formation) of microparticles and microdroplets in the ablated material and a narrow angular distribution of the plasma plume. These drawbacks hamper the formation of uniform films with a high surface area, the films being formed with quite a few defects coming from deposition of coarse particles (droplets) on the substrate.

The presence of microdroplets in the flux of the ablated substance may be due to both removal of microparticles directly from the target under the action of laser radiation and recombination of ionized plasma during expansion. The droplet velocity near the target surface depends on its size and, as a rule, it is much lower than the average velocity of atoms.

In some cases, the size and the number of droplets formed upon ablation from the target surface can be minimized by using dense, for example, crystalline targets with thoroughly polished surfaces.[107, 108, 150, 151] However, in this case, too, it is impossible to fully get rid of microdroplets in the flux of the ablated material. A more tangible result is provided by methods based on the change of deposition geometry (variation of the mutual arrangement of the substrate and the target, the use of baffles, *etc*.).

One way of producing rather homogeneous films by PLD is based on the use of so-called off-axis deposition where the substrate is arranged along the symmetry axis of the propagation of the ablated substance and perpendicular to the target (Fig. 20).[152, 153] The atoms and ions present in the plasma plume are partially deposited on the substrate due to scattering upon collisions in the substance flux and/or in the gas phase, while microdroplets mainly miss the substrate. This arrangement of the substrate relative to the plasma plume results in great non-uniformity of the deposition rate along the film; this, however, can be minimized by using rotating substrates. The off-axis deposition geometry is very sensitive to the mutual arrangement of the substrate and the target and to the position of the target area from which ablation takes place.

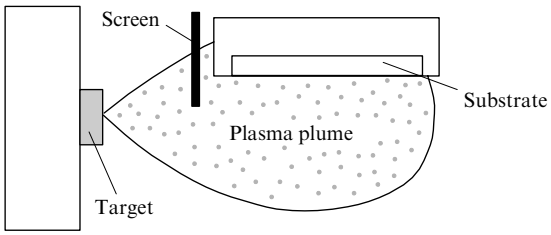


Figure 20. Off-axis deposition geometry.

Since in this case, the substance reactions with the gases in the chamber underlie the deposition, the off-axis geometry is used most often for the PLD in the presence of gases. In some cases, a screen is mounted between the target and the substrate to prevent large particles (clusters and drops) present in the ablated material from hitting the substrate.[154]

Production of rather uniform films with minor amounts of cluster and droplet inclusions is also possible by using two-beam laser vaporization achieved by the formation of cross plasma plumes from two targets located at 90° angle to each other (Fig. 21).[108, 155, 156] The fluxes of ablated material interact with each other and thus deflect from the initial propagation direction. The heavy clusters and droplets are not scattered upon collision of the plumes and do not change the direction of movement. Additional screens prevent them from hitting the substrate. This method provides rather effective control of large particles but medium-size particles still get on the deposited film surface.

A modification of two-beam laser vaporization was proposed by Gyorgy *et al*.,[157, 158] who used two laser radiation sources in the UV and IR range. The numbers of

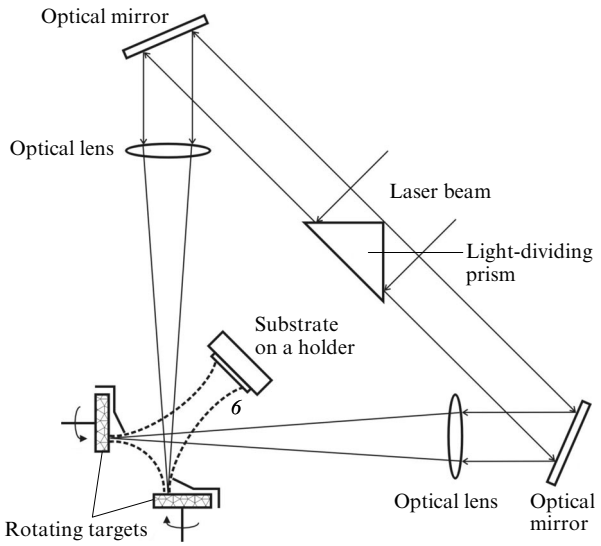


Figure 21. Two-beam laser vaporization

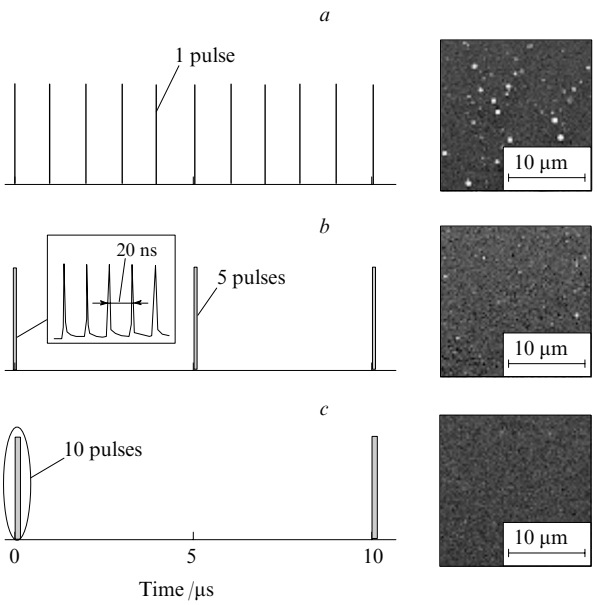


Figure 22. Single pulses at 1 MHz (*a*); a 5-pulse burst at 200 kHz (*b*); a 10-pulse burst at 100 kHz (*c*) and photomicrographs of TiO_2 films (on the right) obtained under the indicated conditions.[159]

macroclusters and droplets on the substrate surface were minimized by their destruction in the flux of ablated material under the action of IR laser radiation directed parallel to the target surface. IR laser pulses have a particular delay relative to the UV laser pulses that induced the ablation. By optimizing the delay time between the pulses and the laser intensities, it is possible to obtain high-quality uniform films deposited in vacuum. If the gas phase is used, it is impossible to completely get rid of microinclusuions in the films by this method.

The use of a succession (burst) of laser pulses can be considered as yet another modification of the two-beam laser vaporization technique. For example, Murakami *et al.*[159] deposited TiO_2 films by means of femtosecond laser radiation in an oxygen atmosphere. The conditions of laser treatment of the target surface were chosen in such a way that the number of pulses per second, the average laser fluence and the pulse energy remained constant in all experiments. The pattern of pulse sequences varied: a single 1 MHz pulse; a 5-pulse burst (20 ns between the pulses), burst frequency 200 kHz; and a 10-pulse burst (20 ns between the pulses), burst frequency 100 kHz. The effect of laser treatment conditions on the quality of deposited films is illustrated in Fig. 22. It can be seen that increase in the number of pulses in the burst leads to decrease in the number and size of the clusters and droplets on the surface of deposited films (by using a 19-pulse burst, a uniform film free from defects and inclusions was obtained). In addition, it was found that the deposition rate increases from 0.05 and 0.25 to 0.33 Å s^{-1}, respectively. The film deposition rate in the PLD method is determined by the pulse energy and the pulse repetition rate. In the given case, these laser radiation parameters remained constant in all experiments. The effect of laser treatment conditions (the use of laser bursts) on the deposition rate attests to complex photophysical processes initiated on the target surface.

A rather efficient way for the control of microparticles may be based on the velocity filtration, because the velocity of ablated species (atoms, ions, clusters, *etc.*) in the flux depends on their mass. In this case, coarse particles can be separated by using a mechanical baffle (Fig. 23). A disc with an orifice rotating at a certain frequency is mounted ahead of the target. The laser beam initiating the ablation hits the target surface after having passed through the orifice of the rotating disc. The disc rotation velocity is specified in such a way that the ablated species that move at a high velocity have time to pass the orifice and reach the substrate surface, while slow droplets and large clusters hit the rotating disc, which thus functions as a protecting screen. This procedure provides high-quality uniform films; however, its technical implementation is rather complex, because it requires feedback systems, synchronization of disc rotation with laser

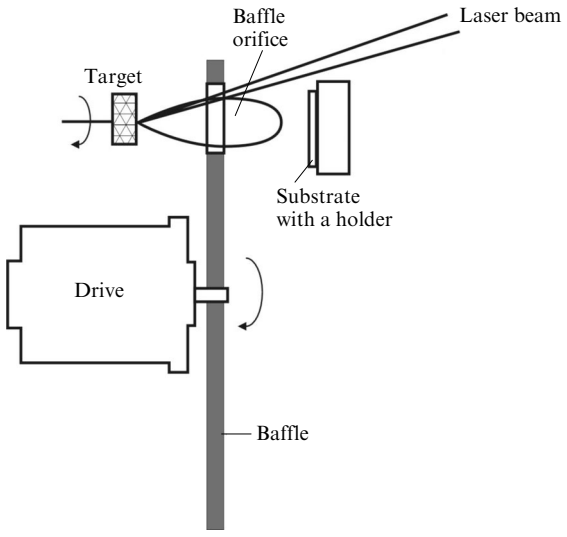


Figure 23. Schematic diagram of the velocity filtration of laser plasma using a mechanical baffle.

pulses and maintenance of a phase lag of the synchronizing pulses.[160–162]

The adverse effects caused by the presence of microdroplets in the ablated flux can be minimized using a simpler experimental implementation of the velocity filtration principle with a target of more intricate design able to rotate at a specified rate (Fig. 24).

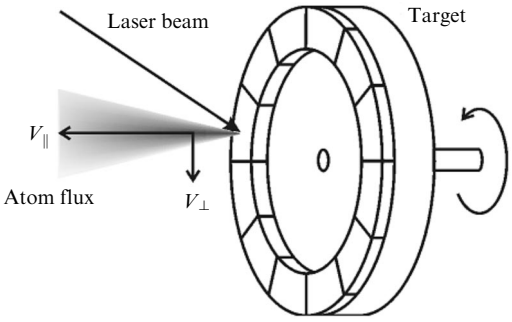


Figure 24. Scheme of the rotating composite target.[163]

When the target rotates, the flux of atoms (and particles) that have taken off from the target surface acquire a linear velocity in the direction perpendicular to the plume expansion. For example, when the target is mounted on a drum with a radius of 20 mm rotating at 4000 rpm, the linear velocity of the ablated material in the direction perpendicular to the plume expansion is ~ 800 cm s^{-1}. Since the velocity of atoms in the flux is high, the $V_{\perp}$ component of the velocity vector adds a negligibly small deviation of the expansion direction from the normal to the target surface. For droplets, which move at a lower velocity than atoms, their velocity being comparable with $V_{\perp}$ in magnitude, this change in the expansion direction may become crucial, so that droplets will no longer hit the substrate.

Experimental studies showed that when the target rotates at 300 rpm, the resulting film has $\sim 20\,000$ droplet defects per square millimetre (Fig. 25 *a*), while at 4000 rpm, the number of observable defects does not exceed 100 per square millimetre (Fig. 25 *b*). The size of accountable droplet defects in a film is from 1 to 10 μm. A photomicrograph of one such defect is shown in Fig. 25 *c*. In the deposition of films using this procedure, the greater part of droplets fall to the bottom of the vacuum chamber (along the rotation direction of the composite target), which is clearly demonstrated by the photographic image of the glass substrate subjected to the ablated material flux (Fig. 25 *d*).

The problem of transverse non-uniformity of the density and chemical composition of the atom flux resulting in non-uniform properties of the deposited films can be solved by averaging the non-uniform distribution of the deposited species, which is attained by rotating the substrate. Nevertheless, the ablated material flux is so narrow that it is often insufficient to rotate the substrate and it is necessary to arrange the substrate at some angle relative to the atom flux direction (Fig. 26).

One more method can be used to enhance the uniformity of properties and compositions of the deposited films. When the revolver rotating drum is used, the targets are attached in such a way that the angle between the normal to the surface of each target and the normals to neighbouring

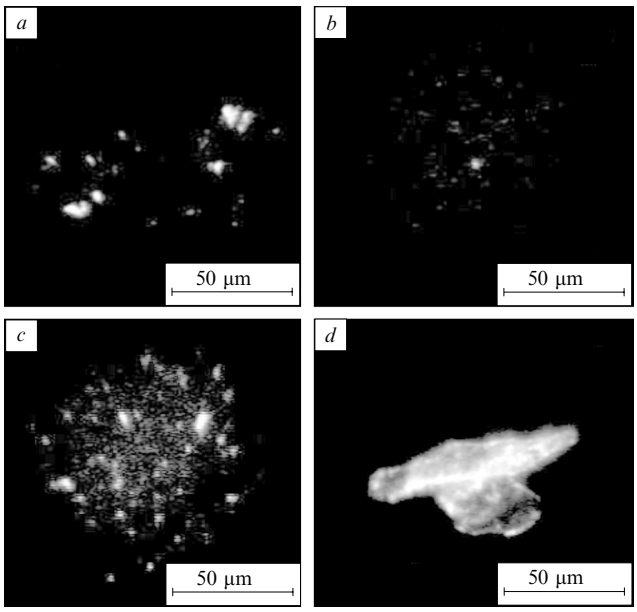


Figure 25. Photomicrographs of film defects. for *a*–*d*, see text.

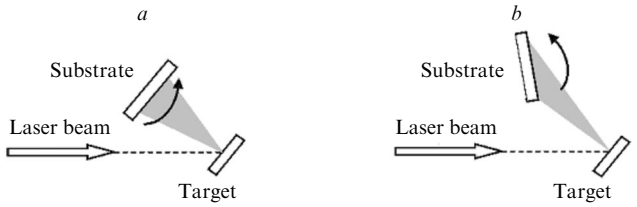


Figure 26. Mutual arrangements of the target and the substrate resulting in a non-uniform film (*a*) and a larger film more uniform in composition and properties (*b*).

targets is 2°. This arrangement provides a wider and more uniform directional pattern of the flux with averaged cross-section distribution parameter of atoms. The schematic views of expansion of atom fluxes ablated from the surface of an ordinary target and from the surface of a rotating composite target are shown in Fig. 27.

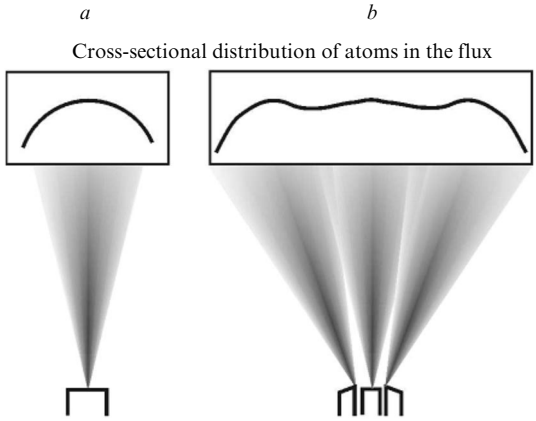


Figure 27. Atom distributions for ordinary (*a*) and composite targets (*b*).

The use of the revolver rotating drum in the PLD technique provides thin films featuring high uniformity of thickness and good optical properties. It was demonstrated, for example, that the deviation of the film thickness in the substrate with 24×24 mm^2 surface area does not exceed 10% (the thickness at the centre of the rotation axis is 1.3 μm, that at a distance of 12 mm from the centre is 1.2 μm). The uniformity of the optical properties over the film area is demonstrated by coincidence of the optical absorption edge positions in different areas of the film. It can be seen in the absorption spectra shown in Fig. 28 that the optical absorption edge positions at the centre and at the periphery of a chalcogenide film obtained by PLD coincide to within the error of the method (442 ± 1 nm).

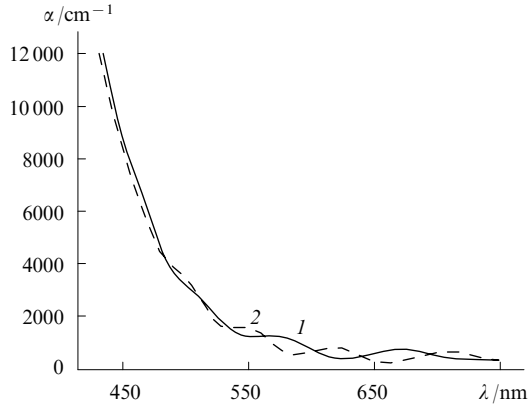


Figure 28. Absorption spectrum at the centre (*1*) and at the periphery (*2*) of chalcogenide film.
α is the optical absorption coefficient.

g. Effect of the substrate properties on the film quality

The substrate type (amorphous or crystalline) and temperature and the state of the surface (defects, oxide film) considerably affect the properties of films obtained by PLD, because all of the above characteristics determine the formation processes of the new phase during condensation of the plasma plume. After an ablated atom or ion reaches the substrate, it is adsorbed on its surface, and subsequently, due to migration over the substrate, they may be either detached or resputtered back to the chamber or may form chemical bonds or be incorporated in the lattice structure.[119] The velocity of migration of adsorbed atoms over the surface is determined by their energy and local environment. An important condition for film formation on a substrate is the mobility of atoms on the surface sufficient for atoms to migrate to thermodynamically favourable positions and to minimize the surface energy. The necessary velocity of atom migration over the surface can be provided by either increasing the substrate temperature or increasing the kinetic energy of ablated particles. However, in both cases, at too high temperatures/energies, there is a probability of adverse effects caused by enhanced diffusion of particles from the surface to the bulk and bulk diffusion, resulting in the formation of structure defects. The energy range of ablated species of 10 – 40 eV is considered to be the optimal for atoms to attain the required velocity of migration over the substrate surface,[119, 164] and the optimal substrate temperature should amount to 0.3 – 0.5 of the melting point of the film being formed.[124]

In the PLD film formation, the selection of the type of substrate is mainly determined by the requirements to film structures. As a rule, for deposition of amorphous films, amorphous substrates are used and crystalline coatings are deposited using crystalline substrates with similar lattice parameters to ensure the epitaxial film growth. Note that even with good correspondence between the crystal lattice parameters of the substrate and the deposited film, the formation of the crystalline phase requires heating of the substrate to a considerable temperature (as a rule, > 500 °C) in order to ensure the sufficient velocity of migration of atoms over the surface. In some cases, to obtain the desired crystal structure of the film, it is annealed at elevated temperature.[165]

It is of interest that under certain conditions (the pressure of the reactive or buffer gas in the deposition chamber and the substrate temperature), an oriented crystalline phase can be synthesized, in particular, on the surface of an amorphous substrate.[166 – 168] For example, it was demonstrated[169] that a ~ 5 nm-thick amorphous phase is formed in the first stage of production of ZnO film on a glass surface at 500 – 600 °C. After the substrate surface has been coated by an amorphous ZnO layer, a 5 – 10 nm-thick polycrystalline ZnO phase is formed. The subsequent film growth affords a *c*-oriented ZnO layer. The possibility of forming an oriented crystalline phase on the surface of an amorphous substrate is apparently related to surface energy and/or internal stress minimization processes.

2. Applications of pulsed laser deposition

As noted above, the advantages of PLD include the possibility of preparation of nanolayered structures and retention of the chemical composition and chemical structure of the target. Consider several examples of application of this method.

a. Films with thermally induced changes in the magnetic state

The spinel $CuCr_2Se_4$ films of about micrometre thick were prepared by PLD.[170] The results of probe analysis confirmed the similarity of the chemical composition of the film to spinel (the deviation was 1% – 2%). According to powder X-ray diffraction data, the films deposited on a cold substrate were amorphous. This was confirmed by measurement of their magnetic susceptibility: the films were not ferromagnetic. In addition, the optical transmission spectra showed that for wavelengths of > 880 nm, the optical absorption coefficient was $< 10^3$ cm^{-1}. Spinel sputtering on the substrate heated to 120 °C gave a film with properties characteristic of the crystalline phase, namely, the dependence of the squared magnetization on the temperature was linear and the optical absorption coefficient was more than 3×10^4 cm^{-1} over the whole range of wavelengths.

Thus, amorphous $CuCr_2Se_4$ layers can be converted to the crystalline state using heat treatment. This conversion is accompanied by crucial change in the magnetic properties (paramagnetic state switches to ferromagnetic state) and optical properties. Heating required for crystallization can be provided by laser radiation.

However, annealing of amorphous films resulted in their destruction due to the arising mechanical stress. In order to avoid the destruction, multilayer films were deposited in

which buffer layers (interlayers between the amorphous spinel layers) were meant to damp the mechanical stress arising upon crystallization. In addition, with this film structure, the size of spinel crystal grains is restricted to the thickness of this layer, and this makes them single-domain. Naturally, it was assumed that the grain dimensions against spatial coordinates are comparable.

Zinc selenide was used as the buffer layer in the deposition of multilayer films. This choice was stipulated by the following requirements. The buffer layer should have high crystallizability; this allows preparing crystalline layers just in the course of deposition without additional heat treatment. Otherwise, during annealing and crystallization, the buffer layer would itself bring about additional mechanical stress. The crystal structure should be highly symmetrical to facilitate thin-layer powder X-ray diffraction. To simplify the multilayer system in question, it is desirable that the layers be formed by one and the same anion (selenide). The crystalline ZnSe has a broad bandgap; therefore, it transmits light in a broad wavelength range, which facilitates the optical investigations of the spinel layers in multilayer structures.

A layered film consisting of 50 $CuCr_2Se_4$ layers (each layer 5 nm thick) separated by 15 nm-thick ZnSe layers was obtained by PLD. The overall film thickness was 1 μm. The scanning electron microscope (SEM) image of the film is shown in Fig. 29. The temperature dependence of the squared magnetization (J^2) of the film is shown in Fig. 30.

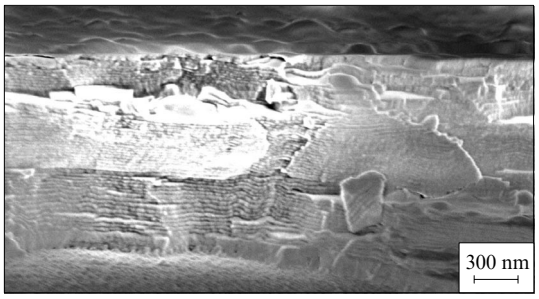


Figure 29. SEM image of a section of the layered $CuCr_2Se_4$/ZnSe film.[140]

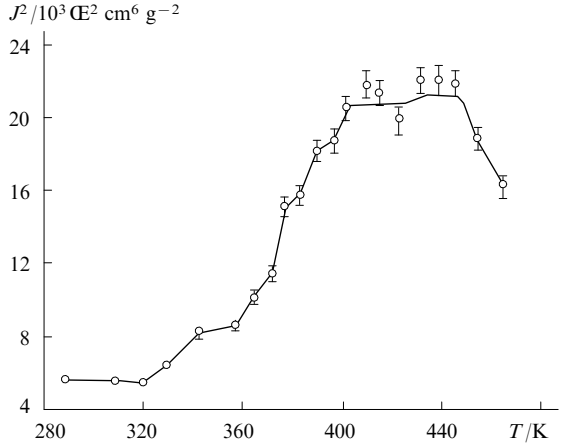


Figure 30. Temperature dependence of the squared magnetization for a multilayer film.[170]

It can be seen that at room temperature, magnetization is vanishingly small, and then, starting from ~340 K, crystallization accompanied by magnetization buildup takes place despite the temperature increase; finally, at ~450 K, magnetization starts to decrease approaching the Curie point. This dependence does not obey the law typical of all ferromagnetic materials, namely, a linear variation *vs.* temperature with a negative slope.

According to magnetic measurements (Fig. 31), the film annealing at 430–450 K for several hours resulted in the spinel phase $CuCr_2Se_4$ with a Curie point of 407 ± 8 K.

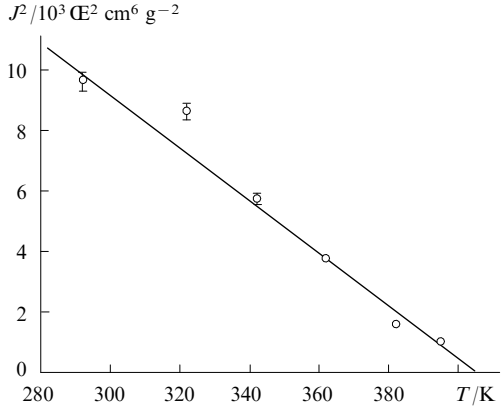


Figure 31. Temperature dependence of the squared magnetization for a multilayer film after annealing.[170]

The amorphous paramagnetic spinel $CuCr_2Se_4$ layers in the film were transferred to the crystalline state in a permanent magnetic field (~200 G) under the action of a Nd : YAG laser radiation at the wavelength of 1 μm and radiation power of 7 W cm^{-2}. The layers thus became ferromagnetic: $J = 60$ Œ cm^3 g^{-1}. This transition was also accompanied by the change in optical transmission. The resulting films can be used for data recording and storage. Data readout can be accomplished using not only magnetic-field sensors but also, apparently, the magneto-optical Faraday effect and a change in the transmission coefficient in the near-IR range.

b. Superionic thin films

The growing demand in superionic materials cannot be satisfied without going beyond classical methods of synthesis.[171] Much is expected of composite electrolytes (both bulk and film ones) with extensive interfacial boundary. When nanolayered films are used in the studies of ion transfer at interfaces, it is possible to monitor the area, length and other parameters of interfaces.

One approach is associated with possible stabilization of the high-temperature AgI phase at lower temperature. The α-AgI phase having high ionic conductivity is known to be stable only above 146 °C, and this markedly restricts the possibility of its practical use. At room temperature and normal atmospheric pressure, two modifications exist, β-AgI with the wurtzite structure and metastable γ-AgI with the sphalerite structure. Upon the α → β transition, the ionic conductivity abruptly decreases by a factor of 10^5.

Presumbly, the high-conductivity ionic phase of silver iodide can be stabilized by alternation of α-AgI nanolayers with nanolayers of another crystalline phase that is stable at room temperature and has a lattice constant of about 5.05 Å (the lattice constant of α-AgI).

As the pairs to AgI for deposition of multilayer films with alternating nanolayers, Ag_2S and Ag_3SI were chosen.[171] The films were deposited on a glass substrate by PLD using an excimer XeCl laser (λ = 308 nm, E_p = 10 mJ, τ_p = 30 ns, ν = 14 Hz). By switching of the laser beam from one target to another with simultaneous use of the laser pulse counting mode for controlling the thickness of the deposited layers, it was possible to produce virtually any multilayer configurations. The targets of two different materials were placed on a metallic disc, which was operated by a microelectric motor to rotate relative to the axis normal to its surface.

In the electron microscope image of a 31-layered structure composed of alternating Ag_3SI and AgI layers (Fig. 32), one can see both nanolayers of different compositions and heterojunctions.

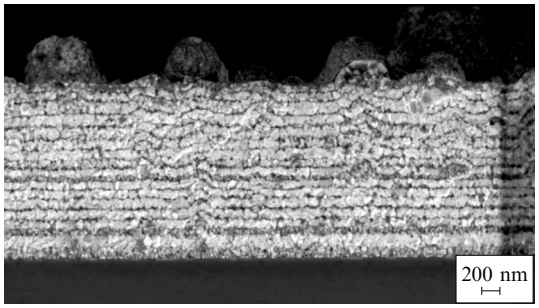


Figure 32. Electron microscope image of the section of a film composed of alternating Ag_3SI and AgI layers (altogether 31 layers).

It was found that[171] multilayer films represent nanostructured media containing three types of inclusions. For Ag_2S- and AgI-based films, these are Ag_2S and AgI inclusions and the Ag_2S/AgI heterojunction. Similarly, for Ag_3SI- and AgI-based films, these are Ag_3SI and AgI inclusions and the Ag_3SI/AgI heterojunction.

According to the data of impedance spectroscopy, the nanolayers in the synthesized films had higher electrical conductivities compared to the electrical conductivities of the equilibrium phases of the same composition at room temperature. The highest electrical conductivities were found for heterojunctions.

The authors failed to confirm the presence of α-AgI by direct methods but the idea to form nanolayers by laser deposition for stabilization of metastable phases is undoubtedly of interest.

It is difficult to preserve the chemical structure and composition of the deposited compound for chalcogenides and especially multicomponent chalcogenides. In particular, this is due to the fact that the saturated vapour pressures of chalcogens are much higher than the saturated vapour pressures of metals and metal-like elements present as parts of compounds and the degrees of dissociation of these compounds upon vaporization are fairly high, especially in the case of ternary compounds. In addition, glass-forming chalcogenides tend to have small differences between the chalcogen–chalcogen, chalcogen–metalloid and metalloid–metalloid chemical bond energies. This further complicates the restoration of the chemical order of the target material on the substrate.

c. Films subject to photoinduced change in the bandgap energy and refractive index

Chalcogenide glasses containing rare earth metal ions are promising luminescence materials for fibre-optics communication systems.[172–174] The thin-film state of these materials is of particular interest. The films of chalcogenide glasses obtained by thermal deposition undergo photostructural transformations and, therefore, they can be used as photoresists, optical switches and memory elements. Combining the thin-film technology and the opportunity of photoinduced control of optical properties appears to be obviously promising. The films obtained by laser deposition occupy a special place.

The glass-like films of different compositions of the $Ga_2S_3-GeS_2$ system both containing and not containing Er^{3+} ions were obtained by PLD.[172–174] The film composition virtually did not depend on the deposition conditions (erbium, gallium and germanium contents were determined) and coincided with the target composition. Unlike magnetron sputtering, the chemical order inherent in the structure of monolithic glass was mainly retained in the film. The Raman spectra of the initial glass and the obtained film of $0.15\,Ga_2S_3-0.85\,GeS_2$ are shown in Fig. 33.

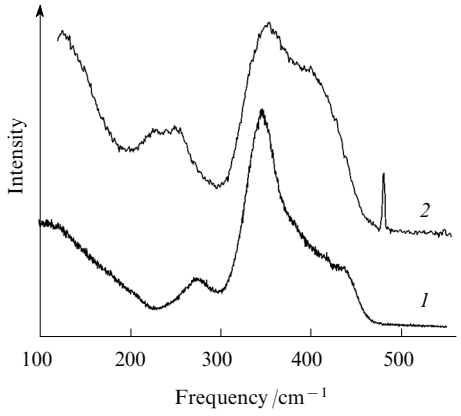


Figure 33. Raman spectra of glass (*1*) and deposited film (*2*) with the composition 0.15 $Ga_2S_3-0.85\,GeS_2$.[173]

The structure of the film, like the glass structure, is determined by the $Ge(Ga)S_{4/2}$ tetrahedra, their fully symmetric vibrations being responsible for the most intense peaks in the absorption spectra (350 cm^{-1}). However, some differences can be noted: in the spectrum of the film, the 280 cm^{-1} peak caused by $S_{3/2}Ge(Ga)-Ge(Ga)S_{3/2}$ vibrations shifts to lower frequency, the scattering intensity at about 400 cm^{-1} increases, and a small narrow peak appears at 485 cm^{-1}, possibly caused by S–S vibrations.

However, some properties (for example, the bandgap energy and refractive index) of the deposited films depended on the deposition conditions. The film absorption edge (for optical absorption coefficient of 10^4 cm^{-1}) deposited onto a cold substrate (without additional heating) shifted to higher

energy relative to the absorption edge of the initial glass, whereas deposition on a heated substrate brought about the opposite effect, namely, a shift to lower energy. The absorption edge position depended also on the deposition rate, which was varied by varying the laser radiation power. An increase in the deposition rate resulted, like the substrate heating, in a long-wavelength shift of the absorption edge (Fig. 34).

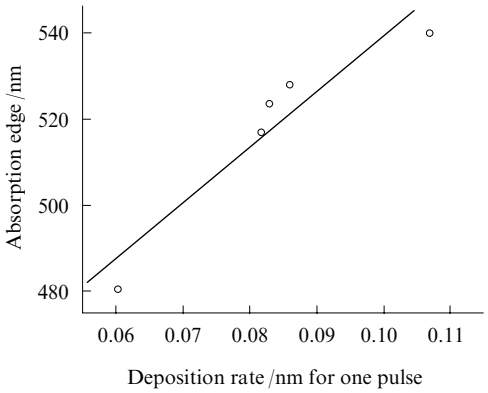


Figure 34. Spectral position of the fundamental absorption edge of films *vs.* deposition rate.
The dots are experimental and the line shows the pattern of dependence.

The increase in the energy of species that condense on the substrate upon its preheating or upon increase in the deposition rate may induce re-evaporation of the more volatile component, in this case, sulfur. The decrease in the sulfur content in the film entails increase in the relative proportion of M—M bonds (M = Ge, Ga). In turn, this should shift the absorption edge to longer wavelengths.

The exposure of a film to the light of a mercury lamp resulted in a pronounced shift of the absorption edge to shorter wavelengths. The magnitude of the shift depended on the absorption edge position for the initial non-irradiated film (Fig. 35 *a*). The photoinduced bleaching was accompanied by a decrease in the refractive index (*n*) (see Fig. 35 *b*).

In addition, the film thickness increased by ~20% upon irradiation. According to the data shown in Fig. 35, the refractive index and the bandgap energy of the irradiated film do not depend on the above parameters of the initial non-irradiated film.

The photoinduced bleaching rate is maximum in the beginning of irradiation. After 20 min, the process arrives at saturation and after 30 min it is almost completed (Fig. 36). The process kinetics is adequately described by the integral form of the first-order reaction kinetics (see the curve in Fig. 36), *i.e.*, the process rate is mainly determined by the concentration of one reaction subject (particular structural defect, particular chemical bond, *etc.*).

Bleaching occurred also when the films were stored in air being exposed to sunlight (the shift was 20 nm in 5 months).

The mechanism of this effect is photoinduced oxidation, as confirmed by vibrational spectroscopy and chemical analysis data. The M—M bond (M = Ge, Ga) reacts with

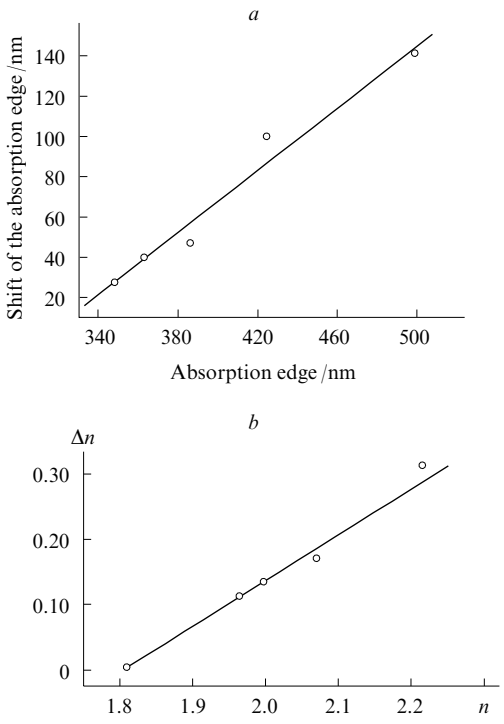


Figure 35. Photoinduced changes in the parameters compared with non-irradiated film parameters.[172]
(*a*) Fundamental absorption edge; (*b*) refractive index. The dots are experimental and the line shows the pattern of dependence.

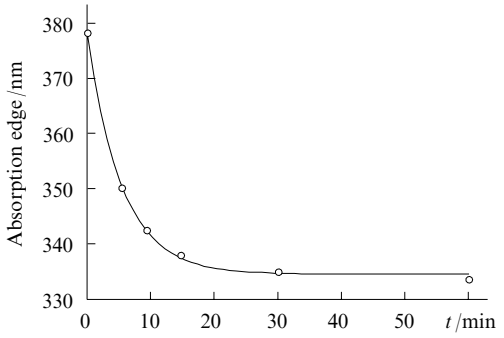


Figure 36. Position of the absorption edge of the film *vs.* irradiation time.[172]
The dots are experimental and the line is approximation with the assumption of the first-order reaction.

oxygen to give M—O—M bridges and the sulfur atom in the ≡Ge(Ga)—S—Ge(Ga)≡ bridges is replaced by oxygen. The photoinduced bleaching mechanism comprises at least two stages separated in time: film irradiation in the absence of oxygen to activate the sites of the subsequent attack by oxygen; the contact of films with air (without irradiation) when oxidation and bleaching processes take place.

The observed photoinduced bleaching effect can be successfully used for one-step recording of images, for example, diffraction gratings or waveguides. A test formation of a diffraction grating in the films was performed. Copying of the diffraction grating in the incident beam

Bragg diffraction mode was used. By means of an N_2 laser, a copy of the transmission grating with 1200 lines per mm was recorded. As the prototype, a grating recorded in the photopolymeric composition deposited onto a quartz substrate was used.

d. Thin film photoabsorbers for solar battery cells

Currently, the polycrystalline semiconductor $Cu_2Se-In_2Se_3$ systems with the chalcopyrite structure are among the most promising photosensitive materials for solar energy conversion. Note that preparation of homogeneous thin films of such semiconductors with specified properties and structure is a challenge. This is due to the large difference between the partial vapour pressures of the components and to existence of a large number of binary and ternary compounds and their polymorphs. Therefore, PLD is expected to offer undeniable advantages compared with the traditional thermal deposition.

By PLD deposition of $CuInSe_2$ on a substrate at room temperature, a glass-like film was obtained.[175–177] Heating of the substrate during deposition resulted in higher fraction of the crystalline phase in the film (Fig. 37 *a*). Heating to $\sim$320 °C is sufficient for complete film crystallization. Meanwhile, increase in the substrate temperature decreased the percentage of selenium in the film and changed the Cu : In content ratio towards increase in the copper percentage (Fig. 37 *b*). The composition was monitored by energy-dispersive spectroscopy.

Thus, to prepare a polycrystalline film, it is necessary to raise the substrate temperature but the chemical composition of the film would be no longer identical to that of the target. To overcome this mismatch, the temperature-and-time pattern of deposition was made more intricate. First, a thin film was deposited onto the cold substrate, then the deposition was interrupted and the substrate temperature was raised to 320 °C in order to crystallize the film, then the substrate temperature was lowered to some temperature '*T*' and the deposition was continued. It was found that to obtain a polycrystalline film, it is necessary to maintain '*T*' at 160–180 °C. This relatively low temperature is due to the fact that deposition was performed on the crystalline surface and no nucleation stage was involved in crystallization. Thus, polycrystalline films with the elemental and phase compositions being the same as the compositions of the $CuInSe_2$ target were obtained.

A similar procedure was developed for the preparation of polycrystalline films of $CuIn_3Se_5$, which also belongs to the $Cu_2Se-In_2Se_3$ system. It was shown that $CuIn_3Se_5$-based films possess electronic conduction, unlike the films obtained from the $CuInSe_2$ target, which possess hole conduction. The bandgap energy for the deposited $CuIn_3Se_5$ films was 1.2 eV (for $CuInSe_2$, this was 1.0 eV), which is much closer to the optimal value for solar light conversion ($\sim$1.4 eV). To study the photosensitivity, the films were deposited onto glass substrates coated by a transparent conducting layer of indium and tin oxides (ITO); graphite served as the second contact. For increasing the photosensitivity, an additional short-term annealing at $\sim$400 °C directly after film deposition without vacuum deterioration was required. The annealed polycrystalline films were well formed (Fig. 38) and demonstrated high photosensitivity (Fig. 39).

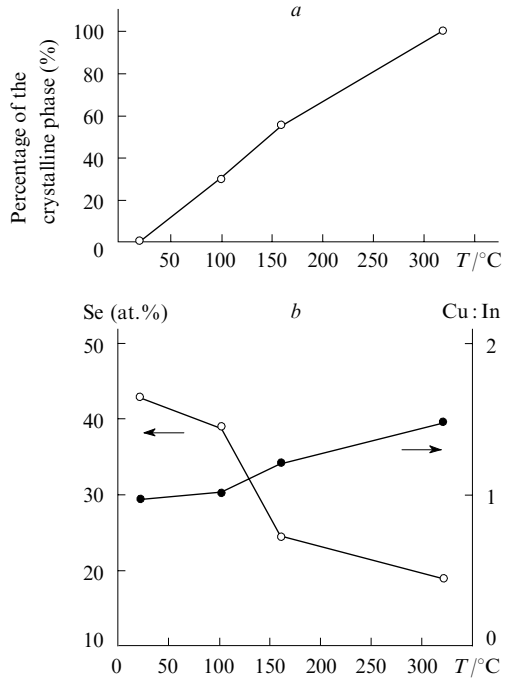


Figure 37. Percentage of the crystalline phase (*a*), selenium content and ratio of copper to indium contents (*b*) in films depending on the substrate temperature.

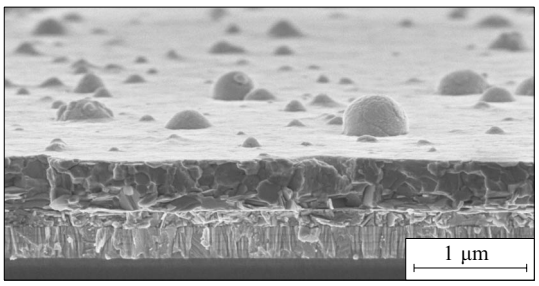


Figure 38. Electron microscope image of a section of the $CuIn_3Se_5$ film.[177]

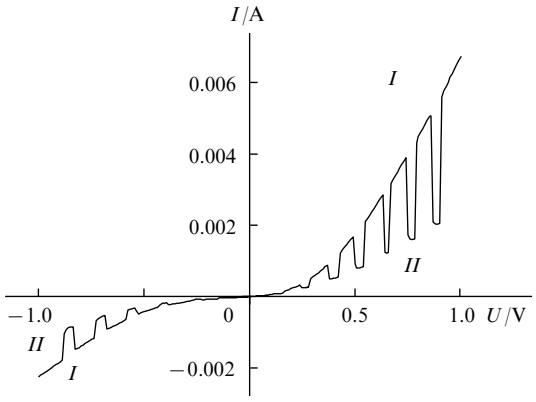


Figure 39. Current – voltage curve of the thin-film structure glass substrate/ITO/$CuIn_3Se_5$/graphite.[177]
Stage: (*I*) in the light, (*II*) in the dark.

The structures based on deposited films (glass substrate/ITO/$CuIn_3Se_5$/graphite) showed almost a diode type current–voltage curve but no charge separation took place on the barrier (on illumination, only photoresistivity changed). The barrier was apparently the Schottky type barrier between $CuIn_3Se_5$ and ITO.

The given examples reflect the possible applications of laser deposition and illustrate its benefits.

IV. Conclusion

The presented analysis of publications devoted to laser ablation in liquid and in vacuum provides the following conclusions. The influence of laser radiation parameters (wavelength, pulse duration and power and treatment duration) is quite multifactorial and can be used to optimize the ablation conditions depending on the particular task. Also, in most cases, for preparing small-size monodisperse particles, it is desirable to use radiation of limiting power at short wavelengths and short pulses.

Generally, it is clear that laser ablation in liquid is technically facile and can be used to obtain a broad range of materials (including multicomponent compounds) in the nanodispersed state without the need to use vacuum equipment. An advantage of the method is also the fact that the nanodispersed substance occurs in a colloid solution and the particle size can be brought down to several nanometres. Therefore, it is very efficient for scientific research. The method is suitable for preparing nanodispersed substances in rather small amounts that are still quite sufficient for the research work.

The applicability to a broad range of materials, versatility and relative simplicity are also characteristics of the laser ablation in vacuum, which is used to obtain thin films. The examples considered in the review, which are far from covering the whole potential applications of laser deposition, do nevertheless illustrate the key advantages of the method; the procedural ease of formation of multilayer structures, including nanosized ones; the correspondence of the elemental composition of the film to the elemental composition of the initial target; the similarity of the phase composition of the film to the phase composition of the initial target. These advantages make pulsed laser deposition highly demanded for the design and manufacture of modern functional film materials for various purposes.

The subsequent studies in this area should be directed, in our opinion, to the exploration of laser ablation under more specific initiation conditions, first of all, using multicolour laser excitation, pulse train excitation, *etc*. This approach will not only provide more in-depth views on the developing ablation mechanisms but also eliminate the existing drawbacks of the method (noticeable nanoparticle size variability, relatively low efficiency of laser ablation), and also this can lead to development of methods for the production of materials with more complex compositions and structures, for example, doped multicomponent nanoparticles, films up to several micrometres thick composed of alternating layers about 10 nanometres thick with sharply different chemical compositions.

References

1. Z Y Jiang, R B Huang, S Y Xie, Z X Xie, L S Zheng *J. Solid State Chem.* **160** 430 (2001)
2. H Su, Y Xie, B Li, Y Qian *Mater. Res. Bull.* **35** 465 (2000)
3. T Tsuji, T Kakita, T Kawamura, J Yamaki, M Tsuji *Chem. Lett.* **33** 1136 (2004)
4. T Tsuji, Y Tatsuyama, M Tsuji, K Ishida, S Okada, J Yamaki *Mater. Lett.* **61** 2062 (2007)
5. J H Ryu, B G Choi, J-W Yoon, K B Shim, K Machi, K Hamada *J. Lumin.* **124** 67 (2007)
6. J H Ryu, S Y Bang, J-W Yoon, C S Lim, K B Shim *Appl. Surf. Sci.* **253** 8408 (2007)
7. F A Krogger *Some Aspects of Luminescence of Solids* (Amsterdam: Elsevier, 1948)
8. R Grasser, A Scharmann *J. Lumin.* **12** 473 (1976)
9. M J Treadway, R C Powell *Phys. Rev. B* **11** 862 (1975)
10. L F Johnson *J. Appl. Phys.* **34** 897 (1963)
11. S Y Wu, H N Dong, W Z Yan, X Y Gao *Phys. Status Solidi B* **241** 1073 (2004)
12. S Baccaro, P Bohacek, A Cecilia, V Laguta, M Montecchi, E Mihokova, M Nikl *Phys. Status Solidi A* **178** 799 (2000)
13. L F Johnson, G D Boyd, K Nassau, R R Soden *Phys. Rev.* **126** 1406 (1962)
14. R Grasser, E Pitt, A Scharmann, G Zimmerer *Phys. Status Solidi B* **69** 359 (1975)
15. D R Shearer, L E Rowe *Med. Phys.* **14** 197 (1987)
16. A Yariv, S P S Porto, K Nassau *J. Appl. Phys.* **33** 2519 (1962)
17. L F Johnson, R A Thomas *Phys. Rev.* **131** 2038 (1963)
18. F Yoshimura, K Nakamura, F Wakai, M Hara, M Yoshimoto, O Odawara, H Wada *Appl. Surf. Sci.* **257** 2170 (2011)
19. G Lin, D Tan, F Luo, D Chen, Q Zhao, J Qiu, Z Xu *J. Alloys Compd.* **507** L43-L46 (2010)
20. T Tsuji, T Hamagami, T Kawamura, J Yamaki, M Tsuji *Appl. Surf. Sci.* **243** 214 (2005)
21. E M Logothesis, K Park, A H Meitzler, K R Laud *Appl. Phys. Lett.* **26** 209 (1975)
22. S K Singh, K Kumar, S B Rai *Mater. Sci. Eng. B* **166** 180 (2010)
23. M Diouf, C Mancini, D Amans, F Chaput, G Ledoux, C Dujardin, in *The 218th ECS Meeting (Abstract 2358)* (Las Vegas, NV: The American Electrochemical Society, 2010) N 5
24. N Acacia, F Barreca, E Barletta, D Spadaro, G Currz, F Neri *Appl. Surf. Sci.* **256** 6918 (2010)
25. G Kiriakidis, M Bender, N Katsarakis, E Gagaoudakis, E Hourdakis, E Douloufakis, V Cimalla *Phys. Status Solidi A* **185** 27 (2001)
26. G Neri, A Bonavita, G Micali, G Rizzo, E Callone, G Carturan *Sens. Actuat. B* **132** 224 (2008)
27. H Steffes, C Imawan, F Solzbacher, E Obermeier *Sens. Actuators B* **78** 106 (2001)
28. T-B Hur, T X Phuoc, M K Chyu *Opt. Laser. Eng.* **47** 695 (2009)
29. T Tsuti, K Iryo, H Ohta, Y Nashimura *Jpn. J. Appl. Phys.* **39** L981 (2000)
30. R A Ganeev, A I Ryasnyansky *Opt. Commun.* **246** 163 (2005)
31. R A Ganeev, A I Ryasnyanskiy, T Usmanov *Opt. Commun.* **272** 242 (2007)
32. A A Lalayan *Appl. Surf. Sci.* **248** 209 (2005)
33. V Svrcek, M Kondo *Appl. Surf. Sci.* **255** 9643 (2009)
34. O R Musaev, J M Wrobel, D M Wieliczka, V Dusevich, M B Kruger *Physica E* **40** 3147 (2008)

35. R D Schaller, V I Klimov *Phys. Lett* **92** 186601 (2004)
36. R J Ellingson, M C Beard, J C Johnson, P Yu, O I Micic, A J Nozik, A Shabaev, A I Efros *Nano Lett*. **5** 865 (2005)
37. S A McDonald, G Konstantatos, S Zhang, P W Cyr, E J D Klem, L Levina, E H Sargent *Nature Mater*. **4** 138 (2005)
38. M T Harrison, S V Kershaw, M G Burt, A I Rogach, A Kornowski, A Eychmuller, H Weller *Pure Appl. Chem*. **72** 295 (2000)
39. D V Talapin, C B Murray *Science* **310** 86 (2005)
40. C Chubilleau, B Lenoir, S Migot, A Dauscher *J. Colloid Interface Sci*. **357** 13 (2011)
41. H W Kroto, J R Heath, S C O'Brein, R F Curl, R E Smalley *Nature (London)* **318** 162 (1985)
42. T Guo, P Nikolaev, A Thess, D T Colbert, R E Smalley *Chem. Phys. Lett*. **243** 49 (1995)
43. J R Heath, Q C O'Brien, R F Curl, H W Kroto, R E Smalley *J. Am. Chem. Soc*. **109** 359 (1987)
44. M Tsuji, T Tsuji, S Kuboyama, S-H Yoon, Y Korati, T Tsujimoto, K Kubo, A Mori, I Mochida *Chem. Phys. Lett*. **355** 101 (2002)
45. M Tsuji, S Kuboyama, T Matsuzaki, T Tsuji *Carbon* **41** 2141 (2003)
46. H Tabata, M Fujii, S Hayashi *Carbon* **44** 522 (2006)
47. H Tabata, M Fujii, S Hayashi *Chem. Phys. Lett*. **395** 138 (2004)
48. J Hobley, T Nakamori, S Kajimoto, M Kasuya, K Hatanaka, H Fukumura, S Nishio *J. Photochem. Photobiol., A* **189** 105 (2007)
49. Y Tamaki, T Asahi, H Masuhara *Appl. Surf. Sci*. **168** 85 (2000)
50. Y Tamaki, T Asahi, H Masuhara *J. Phys. Chem. A* **106** 2135 (2002)
51. Y Tamaki, T Asahi, H Masuhara *Jpn. J. Appl. Phys*. **42** 2725 (2003)
52. B Li, T Kawakami, M Hiramatsu *Appl. Surf. Sci*. **210** 17 (2003)
53. M Boutinguiza, F Lusquinos, R Comesana, A Riveiro, F Quintero, J Pou *Appl. Surf. Sci*. **254** 1264 (2007)
54. M Boutinguiza, F Lusquinos, A Riveiro, R Comesana, J Pou *Appl. Surf. Sci*. **255** 5382 (2009)
55. M Boutinguiza, J Pou, F Lusquiños, R Comesaña, A Riveiro *Appl. Surf. Sci*. **257** 5195 (2011)
56. M Boutinguiza, J Pou, F Lusquiños, R Comesaña, A Riveiro *Phys. Proc*. **12** 54 (2011)
57. T Sakka, K Saito, Y H Ogata *Appl. Surf. Sci*. **197** 246 (2002)
58. G W Yang *Prog. Mater. Sci*. **52** 648 (2007)
59. L Berthe, A Sollier, R Fabro, P Peyer, E Bartnicki *J. Phys. D* **33** 2142 (2000)
60. P Peyer, L Berthe, R Fabbro, A Sollier *J. Phys. D* **30** 498 (2000)
61. L Yang, P W May, L Yin, J A Smith, K N Rosser *Diamond Relat. Mater*. **16** 725 (2007)
62. J B Wang, C Y Zhang, X L Zhong, G W Yang *Chem. Phys. Lett*. **361** 86 (2002)
63. J B Wang, G W Yang *J. Phys.: Condens. Matter* **11** 7089 (1999)
64. K Saito, K Takatani, T Sakka, Y H Ogata *Appl. Surf. Sci*. **197**–**198** 56 (2002)
65. B Kumar, R K Soni *Mater. Chem. Phys*. **121** 95 (2010)
66. In *Cohesive Properties of Semiconductors under Laser Irradiation (NATO ASI Series)* (Ed. I D Laude) (Hague: Martinus Nijhoff Publ., 1983) p. 71
67. H Liu, F Chen, X Wang, Q Yang, H Bian, J Si, X Hou *Thin Solid Films* **518** 5188 (2010)
68. G Daminelli, J Kruger, W Kautek *Thin Solid Films* **467** 334 (2004)
69. S Besner, J Y Degorce, A V Kabashin, M Meunier *Appl. Surf. Sci*. **247** 163 (2005)
70. A Borowiec, H F Tiedje, H K Haugen *Appl. Surf. Sci*. **243** 129 (2005)
71. N G Semaltianos, S Logothetidis, N Frangis, I Tsiaoussis, W Perrie, G Dearden, K G Watkins *Chem. Phys. Lett*. **496** 113 (2010)
72. Z Yan, R Bao, D B Chrisey *Nanotechnology* **21** 145609 (2010)
73. E Stratakis, M Barberogloum C Fotakis, G Viau, C Garcia, G A Shafeev *Opt. Express* **17** 12650 (2009)
74. A A Ruth, J A Young *Colloids Surf. A* **279** 121 (2006)
75. M Nath, C N R Rao, R Popovitz-Biro, A Albu-Yaron, R Tenne *Chem. Mater*. **16** 2238 (2004)
76. H Aleali, L Sarkhosh, R Karimzadeh, N Mansour *Phys. Status Solidi B* **248** 680 (2011)
77. S J Henley, S Mollah, C E Giusca, S R P Silva *J. Appl. Phys*. **106** 064309 (2009)
78. V Kosalathip, T Kumpeerapun, S Migot, B Lenoir, A Dauscher *Adv. Mater. Res*. **55**–**57** 809 (2008)
79. V Švrček *Pure Appl. Chem*. **80** 2513 (2008)
80. V Švrček, M Kondo, K Kalia, D Mariotti *Chem. Phys. Lett*. **478** 224 (2009)
81. V Kosalathip, A Dauscher, B Lenoir, S Migot, T Kumpeerapun *Appl. Phys. A* **93** 235 (2008)
82. C Candolfi, A Thiam, B Lenoir, A Dauscher, in *Proceedings of the 2nd European Conference on Thermoelectricity, Cracovie, 2004*
83. H Grisaru, O Palchik, A Gedanken, V Palchik, A M Weiss, M A Slifkin *Inorg. Chem*. **42** 22 (2003)
84. T Sasaki, Y Shimizu, N Koshizaki *J. Photochem. Photobiol. A* **182** 335 (2006)
85. T Tsuji, K Iryo, Y Nishimura, M Tsuji *J. Photochem. Photobiol. A* **145** 201 (2001)
86. A Fojtik, A Henglein *Ber. Busen-Ges. Phys. Chem*. **97** 252 (1993)
87. C Liang, Y Shimizu, T Sasaki, N Koshinaki *J. Phys. Chem. B* **107** 9220 (2003)
88. C Liang, T Sasaki, Y Shimizu, N Koshinaki *Chem. Phys. Lett*. **389** 59 (2004)
89. P P Patil, D M Phase, S A Kulkarni, S V Ghaisas, S K Kulkimi, S M Kanetkar, S B Ogate, V G Bhide *Phys. Rev. Lett*. **58** 238 (1987)
90. K V Ankin, N N Melnik, A V Simakin, G A Shafeev, V V Voronov, A G Vitukhonovsky *Chem. Phys. Lett*. **366** 357 (2002)
91. M S Yeh, Y S Yang, Y P Lee, H F Lee, Y H Yeh, C S Yeh *J. Phys. Chem*. **103** 6851 (1999)
92. T X Phuoc, B H Howard, D V Martello, Y Soong, M K Chyu *Opt. Lasers Eng*. **46** 829 (2008)
93. F Mafune, T Kondow *Chem. Phys. Lett*. **343** 383 (2004)
94. C H Bae, S H Nam, S M Park *Appl. Surf. Sci*. **197**–**198** 623 (2002)
95. F Mafune, J Kohno, Y Takeda, T Kondow *J. Phys. Chem. B* **104** 9111 (2000)
96. S S Kher, R L Wells *Chem. Mater*. **6** 2056 (1994)
97. H Yao, S Takahara, H Mizuma, T Kosegi, T Hayashi *Jpn. J. Appl. Phys*. **35** 4633 (1996)
98. R A Ganeev, A I Ryasnyansky, M K Kodirov, S R Kamalov, V A Li, R A Tugushev, T Usmanov *Appl. Phys. B* **74** 47 (2002)
99. H Fujiwara, S Yanagida, P V Kamat *J. Phys. Chem. B* **103** 2589 (1999)
100. A Amendola, M Megenhetti *Phys. Chem. Chem. Phys*. **11** 3805 (2009)
101. S I Dolgaev, M E Karasev, L A Kulevskii, A V Simakin, G A Shafeev *Kvant. Elektron*. **31** 593 (2001) [a]
102. A Nath, S S Laha, A Khare *Appl. Surf. Sci*. **257** 3118 (2011)
103. Zh L Wang, Y Liu, Z Zhang, *Handbook of Nanophase and Nanostructured Materials* (Dordrecht: Kluwer Academic, Plenum, 2003)
104. *Laser Ablation and its Applications* (Ed. P Claude) (Berlin: Springer, 2007)
105. E Sharon *Black Laser Ablation: Effects and Applications* (New York: Nova, 2011)

106. K L Saenger, in *Pulsed Laser Deposition of Thin Films* (Eds D B Chrisey, G K Hubler) (New York: Wiley Interscience, 1994)
107. R Eason *Pulsed Laser Deposition of Thin Films: Applications-Led Growth of Functional Materials* (New York: Wiley Interscience, 2007)
108. H-U Krebs, M Weisheit, J Faupel, E Suske, T Scharf, Ch Fuhse, M Stormer, K Sturm, M Seibt, H Kijewski, D Nelke, E Panchenko, M Buback *Adv. Solid State Phys.* **43** 505 (2003)
109. S Pessaud, M Licheron, F Gervais, C Champeaux, P Marchet, A Catherinot *Proc. SPIE* **3404** 116 (1998)
110. M S Hegde *Proc. Indian Acad. Sci. (Chem. Sci.)* **113** 445 (2001)
111. R Delmdahl, R Patzel *Appl. Phys. A* **93** 611 (2008)
112. H M Smith, A F Turner *Appl. Opt.* **4** 147 (1965)
113. H Schwarz, H A Tourtellotte *J. Vac. Sci. Technol.* **6** 373 (1969)
114. G Hass, J B Ramsey *Appl. Opt.* **8** 1115 (1969)
115. Y A Bykovskii *Sov. Phys. Tech. Phys.* **23** 578 (1978)
116. S I Anisimov, B S Luk'yanchuk *Usp. Fiz. Nauk* **172** 301 (2002) [b]
117. E N Sobol *Phase Transformations and Ablation in Laser-Treated Solids* (New York: Wiley, 1995)
118. B C Stuart, M D Feit, A M Rubenchik, B W Shore, M D Perry *Phys. Rev. Lett.* **74** 2248 (1995)
119. P R Willmott, J R Hube *Rev. Mod. Phys.* **72** 315 (2000)
120. X Zenga, X Mao, R Greif, R E Russo *Proc. SPIE* **5448** 1150 (2004)
121. D Waller, L G Coccia, J A Kilner, I W Boyd *Solid State Ionics* **134** 119 (2000)
122. C Ristoscu, E Gyorgy, I N Mihailescu, A Klini, V Zorba, C Fotakis *Appl. Phys. A* **79** 927 (2004)
123. E Gyorgy, C Ristoscu, I N Mihailescu, A Klini, N Vainos, C Fotakis, C Ghica, G Schmerber, J Faerber *J. Appl. Phys.* **90** 456 (2001)
124. P R Willmott *Prog. Surf. Sci.* **76** 163 (2004)
125. M Liu, B Mana, X Lin, X Li *J. Crystal Growth* **311** 1087 (2009)
126. B Y Man, H Z Xi, C S Chen, M Liu, J Wei *Cent. Eur. J. Phys.* **6** 643 (2008)
127. D T Peeler, P T Murray *Diamond Relat. Mater.* **3** 1124 (1994)
128. A Szekeres, S Simeonov, S Bakalova, I Minkov, A Cziraki, C Ristoscu, G Sokol, G Dorcioman, I N Mihailescu *J. Optoelectron. Adv. Mater.* **12** 542 (2010)
129. M Stormer, H-U Krebs *J. Appl. Phys.* **78** 7080 (1995)
130. S Kahl, H-U Krebs *Phys. Rev. B* **63** 172103 (2001)
131. E Treece, J S Horwitz, S B Qadri, E F Skelton, E P Donovan, D B Chrisey *J. Solid State Chem.* **117** 294 (1995)
132. S K Hau, K H Wong, P W Chan, C L Choy *Appl. Phys. Lett.* **66** 245 (1995)
133. S Fähler, K Sturm, H-U Krebs *Appl. Phys. Lett.* **75** 3766 (1999)
134. K Sturm, H-U Krebs *J. Appl. Phys.* **90** 1061 (2001)
135. K Sturm, S Fähler, H-U Krebs *Appl. Surf. Sci.* **154–155** 462 (2000)
136. T Scharf, H-U Krebs *Appl. Phys. A* **75** 551 (2002)
137. T Scharf, J Faupel, K Sturm, H-U Krebs *J. Appl. Phys.* **94** 4273 (2003)
138. G M Matenoglou, G A Evangelakis, C Kosmidis, P Patsalas *Rev. Adv. Mater. Sci.* **15** 38 (2007)
139. J M Lackner, W Waldhauser, R Ebner, M Beutl, G Jakopic, G Leising, H Hutter, M Rosner *Appl. Phys. A* **79** 1525 (2004)
140. M Rusop, S M Mominuzzaman, T Soga, T Jimbo, M Umeno *Asian J. Energy Environ.* **5** 309 (2004)
141. V Yu Fominski, A M Markeev, V N Nevolin, V B Prokopenko, A R Vrublevski *Thin Solid Films* **248** 240 (1994)
142. A V Gusarov, A G Gnedovets, I Smurov *J. Appl. Phys.* **88** 4352 (2000)
143. J Škriniarová, J Kovác, D Haško, A Vincze, J Jakabovic, L Jánoš, M Veselý, I Novotný, J Bruncko *J. Phys.: Conf. Ser.* **100** 042031 (2008)
144. A Kühle, J L Skov, S Hjorth, I Rasmussen, J Bindslev Hansena *Appl. Phys. Lett.* **64** 3178 (1994)
145. M Walczak, M Oujja, J F Marco, M Sanz, M Castillejo *Appl. Phys. A* **93** 735 (2008)
146. H Luna, D F Franceschini, R Prioli, R B Guimarães, C M Sanchez, G P Canal, M D L Barbosa, R M O Galvão *J. Vac. Sci. Technol., A* **28** 1092 (2010)
147. X Y Chen, Y F Lu, Y H Wu, B J Cho *J. Appl. Phys.* **96** 3180 (2004)
148. A Gupta, B W Hussey, M Y Chern *Physica C* **200** 263 (1992)
149. P R Willmott, R Timm, J R Huber *J. Appl. Phys.* **82** 2082 (1997)
150. C Scarfone, M G Norton, C B Carter, J Li, H W Mayer *Mater. Res. Soc. Symp. Proc.* **191** 183 (1991)
151. S Fahler, M Stormer, H-U Krebs *Appl. Surf. Sci.* **109–110** 433 (1997)
152. B Holzapfel, B Roas, L Schultz, P Bauer, G Saemann-Ischenko *Appl. Phys. Lett.* **61** 3178 (1992)
153. J H Kim, K A Jeon, H S Kang, S Y Lee *Superlattices Microstruct.* **39** 60 (2006)
154. E Kaidashev, V Dneprovski, D Breus, R N Sheftal *J. Supercond.* **13** 407 (2000)
155. A A Gorbunov, W Pompe, A Sewing, S V Gaponov, A D Akhsakhalyan, I G Zabrodin, I A Kaskov, E B Klyenkov, A P Morozov, N N Salaschenko, R Dietsch, H Mai, S Vollmar *Appl. Surf. Sci.* **96–98** 649 (1996)
156. T Schauer, L Weber, J Hafner, O Kus, E V Pechen, A V Varlashkin, T Kaiser, K F Renk *Supercond. Sci. Technol.* **11** 270 (1998)
157. E Gyorgy, I N Mihailescu, M Kompitsas, A Giannoudakos *Appl. Surf. Sci.* **195** 270 (2002)
158. E Gyorgy *Thin Solid Films* **446** 178 (2004)
159. M Murakami, B Liu, Zh Hu, Zh Liu, Y Uehara, Y Che *Appl. Phys. Express* **2** 042501 (2009)
160. E V Pechen, A V Varlashkin, S I Krasnosvobodtsev, B Brunner, K F Renk *Appl. Phys. Lett.* **66** 2292 (1995)
161. E V Pechen, A V Varlashkin, S I Krasnosvobodtsev, K F Renk *Czech. J. Phys.* **46** 1509 (1996)
162. E V Pechen, A V Varlashkin, A I Golovashkin *Physica B* **284–288** 1025 (2000)
163. E N Borisov, Ya G Grigor'ev, T Yu Ivanova, A V Kurochkin, A A Manshina, A V Povolotskii, in *Lazernye Issledovaniya v Sankt-Peterburgskom Gosudarstvennom Universitete* (Laser Investigations in Saint Petersburg State University) (St Petersburg: St Petersburg State University, 2004) Vol. 3, p. 220
164. D K Brice, J Y Tsao, S T Picraux *Nucl. Instrum. Methods Phys. Res. B* **44** 68 (1989)
165. L S Hsu, D Lucaa *J. Optoelectron. Adv. Mater.* **5** 841 (2003)
166. S Tiwari, R Prakash, R J Choudhary, D M Phase *J. Phys. D: Appl. Phys.* **40** 4943 (2007)
167. Sh Zhu, D H Lowndes, J D Budai, D P Norton *Appl. Phys. Lett.* **65** 2012 (1994)
168. Y H Yu, M O Lai, L Lu *Appl. Phys. A* **88** 365 (2007)
169. S Hayamizua, H Tabata, H Tanaka, T Kawai *J. Appl. Phys.* **80** 787 (1996)
170. D S Kim, A N Rusnak, Yu S Tveryanovich, O Volobujeva, M Kim, S Kwon *Fiz. Khim. Stekla* **34** 189 (2008) [c]
171. Yu S Tveryanovich, M D Bal'makov, V V Tomaev, E N Borisov, O Volobujeva *Fiz. Khim. Stekla* **34** 196 (2008) [c]
172. A S Tverjanovich, E N Borisov, O A Sokolova, Yu S Tveryanovich *Fiz. Khim. Stekla* **31** 235 (2005) [c]

173. A S Tverjanovich, E N Borisov, O Volobueva, S B Mamedov, M D Mikhailov *Fiz. Khim. Stekla* **32** 930 (2006) [c]
174. A Tverjanovich, A Kotikova, E N Borisov *Laser Phys. Lett.* **4** 341 (2007)
175. A S Tverjanovich, E N Borisov, E S Vasilieva, O V Tolochko, I E Vahhi, S Bereznev, Yu S Tveryanovich *Solar Energy Mater. Solar Cells* **90** 3624 (2006)
176. E N Borisov, Ya Vertsimakha, P Lutsik, A S Tverjanovich, Yu S Tveryanovich *Fiz. Tekh. Poluprovod.* **41** 1414 (2007) [d]
177. A Tverjanovich, S Bereznev, E N Borisov, D Kim, J Kois, K Laes, O Volobujeva, A Opik, E Mellikov, Yu Tveryanovich *Proc. Eston. Acad. Sci.* **58** (1) 24 (2009)

[a] — *Quant. Electron. (Engl. Transl.)*
[b] — *Physics-Uspekhi (Engl. Transl.)*
[c] — *Glass Phys. Chem. (Engl. Transl.)*
[d] — *Semiconductors (Engl. Transl.)*